Master's Thesis

Small Molecules as Chemical Tools for Regulation of Metal-Amyloid-β Aggregation

Yonghwan Ji

Department of Chemistry

Graduate School of UNIST

2018

Small Molecules as Chemical Tools for Regulation of Metal-Amyloid-β Aggregation

Yonghwan Ji

Department of Chemistry

Graduate School of UNIST

Small Molecules as Chemical Tools for Regulation of Metal-Amyloid-β Aggregation

A thesis submitted to the Graduate School of UNIST
in partial fulfillment of the requirements
for the degree of Master of Science

Yonghwan Ji

12. 05. 2017

Approved by

Advisor
Associate Professor Mi Hee Lim

Small Molecules as Chemical Tools for Regulation of Metal-Amyloid-β Aggregation

Yonghwan Ji

This certifies that the thesis of Yonghwan Ji is approved.

12. 05. 2017

Signature

Advisor: Associate Professor Mi Hee Lim

Signature

Associate Professor Cheol-Min Park

Signature

Associate Professor Wonyoung Choe

Abstract

Alzheimer's disease (AD) is most common form of dementia. Symptomatically, memory loss and cognitive decline is observed. In 2016, more than 33 million people worldwide are suffered from AD. The complexity of AD, however, stems from the inter-relation of multiple pathological factors upon initiation and progression of the disease. For example, the amyloid-β (Aβ) peptides aggregate toward bigger species and form the senile plaque in AD brain. The high concentration of metal ions [*e.g.*, Cu(I/II), Zn(II), and Fe(II/III)] are observed in this senile plaques. Metal ions also could bind to Aβ and show different properties with metal-free Aβ. Additionally, from these redox active metal ions [*e.g.*, Cu(I/II) and Fe(II/III)], could overproduce the reactive oxygen species (ROS) through Fenton-like reactions. To identify the involvement of metal-bound amyloid-β (metal–Aβ) aggregation in AD pathology, small molecules as chemical tools capable of controlling metal–Aβ aggregation have been developed. Herein, we describe the design of small molecules as chemical tools to target metal–Aβ. Introduction of hypotheses of the AD and previous reported chemical tools for metal–Aβ in Chapter 1, and 2,2'-bipyridine (**bpy**) derivatives (**1**–**4**) rationally designed to be chemical modulators towards metal–Aβ aggregation over metal-free Aβ analog will be described in Chapter 2. Additionally, design molecule to inhibit the transcription factor, ΔFosB are proposed in Appendix A. Overall, our studies of the **bpy** derivatives demonstrate that the alteration of metal binding properties as well as the installation of an Aβ interacting capability onto a metal chelating framework, devised *via* the rational structure-based design, were able to achieve evident modulating reactivity against metal–Aβ aggregation. Obviating the need for complicated structures, our design approach could be appropriately utilized for inventing small molecules as chemical tools for studying desired metal-related targets in biological systems.

Table of Contents

List of Tables

List of Figures

Figure 2.6. ESI-MS spectra of $A\beta_{40}$ incubated with excess amounts of compounds (**bpy**, **1**, and **4**) in the absence and presence of Cu(II). ESI-MS spectra of $A\beta_{40}$ without (a) and with (b) Cu(II). Conditions: $[A\beta_{40}]$ = 100 μM; $[CuCl_2]$ = 100 μM; [compound] = 500 μM; 20 mM ammonium acetate, pH 7.2 (1% v/v DMSO); 37 °C; 1 h incubation; no agitation; 10-fold diluted samples were injected to the mass spectrometer. (c) Tandem MS (ESI-MS^2) spectrum of the +4-charged ternary complex ($[A\beta_{40}$ + Cu(II) + **1** + $2H]^{4+}$, 1148 *m/z*). The ESI-MS^2 results support the formation of a ternary complex composed of $A\beta_{40}$, Cu(II), and **1**. The relative abundance of each spectrum was individually normalized based on the highest peak.

Figure 2.7. Tandem MS (ESI-MS^2) spectrum of the +4-charged peak at 1151 *m/z* from the sample containing $A\beta_{40}$, Cu(II), and **4**. The ESI-MS^2 results supported that the peak was assigned to $[A\beta + 2Cu + 2K + 4H_2O - 2H]^{4+}$, thus indicating no formation of a ternary complex composed of $A\beta_{40}$, Cu(II), and **4**. Conditions: $[A\beta_{40}]$ = 100 μM; $[CuCl_2]$ = 100 μM; [compound] = 500 μM; 20 mM ammonium acetate, pH 7.2 (1% v/v DMSO); 37 °C; 1 h incubation; no agitation; the 10-fold diluted samples were injected to the mass spectrometer. The relative abundance of each spectrum was individually normalized based on the highest peak.

Figure 2.8. Effects of **bpy** and **1**–**4** towards formation of metal-free Aβ and metal–Aβ aggregates. (a) Scheme of the experiments. (b) Visualization of the resultant $A\beta_{40}$ and $A\beta_{42}$ species by gel electrophoresis with Western blotting (gel/Western blot) using an anti-Aβ antibody (6E10). Conditions: [Aβ] = 25 μM; [$CuCl_2$ or $ZnCl_2$] = 25 μM; [compounds] = 50 μM; 24 h; pH 6.6 (for Cu(II)-treated experiments) or pH 7.4 (for metal-free and Zn(II)-added experiments); 37 °C; constant agitation. Lanes: (**C**) [Aβ (± $CuCl_2$ or $ZnCl_2$)]; (**B**) [(C) + **bpy**]; (**1**) [(C) + **1**]; (**2**) [(C) + **2**]; (**3**) [(C) + **3**]; (**4**) [(C) + **4**]. (c) TEM images of the 24 h incubated $A\beta_{40}$ samples from (b) [the TEM images of the resultant $A\beta_{42}$ aggregates from (b) are presented in Figure 2.9]. The insets represent the minor species. Scale bar = 200 nm.

Figure 2.9. TEM images of the resultant metal-free $A\beta_{42}$ and metal–$A\beta_{42}$ aggregates generated upon treatment with **bpy** and **1**–**4**. (a) Scheme of the experiments. (b) TEM images of the 24 h incubated $A\beta_{42}$ samples from Figure 2.8. Scale bar = 200 nm.

Figure 2.10. Toxicity of **bpy** and **1**–**4** in SH-SY5Y cells. Cells were treated with **bpy** or **1**–**4** for 24 h at 37 °C. Cell viability (%) was determined by the MTT assay. The viability values were calculated

compared to those of cells added with DMSO only (1%, v/v). Error bars represent the standard error from three independent experiments ($P < 0.05$).

Figure 2.11. Toxicity of **bpy** and **1**–**4** in SH-SY5Y cells in the presence of metal ions. Cells were treated with **bpy** or **1**–**4** (10 μM) with metal ions (5 or 10 μM) for 24 h at 37 °C. Cell viability (%) was determined by the MTT assay. The viability values of cells were calculated compared to those of cells added with DMSO only (1%, v/v). Error bars represent the standard deviation from three independent experiments ($P < 0.05$).

Figure A.1. ^{1}H NMR spectrum of **C6-OH** [400 MHz, $(CD_3)_2SO$]

Figure A.2. ^{1}H NMR spectrum of **C6-OK** [400 MHz, $(CD_3)_2SO$]

Figure A.3. ^{1}H NMR spectrum of **C6-n2m** [400 MHz, $(CD_3)_2SO$]

Figure A.4. ^{13}C NMR spectrum of **C6-OK** [100 MHz, $(CD_3)_2SO$]

Figure A.5. ^{1}H NMR spectrum of **C6-n4m'** [400 MHz, $(CD_3)_2SO$]

Figure A.6. ^{13}C NMR spectrum of **C6-n4m'** [100 MHz, $(CD_3)_2SO$]

List of Schemes

List of Abbreviations

8-HQ	8-hydroxyquinline
Aβ	Amyloid-β
AD	Alzheimer's disease
APP	Amylid precursor protein
BBB	Blood-brain barrier
bpy	2,2'-bipyridine
BSA	Bovine serum albumin
CNS	Central nervous system
CQ	Clioquinol; 5-chloro-6-iodoqunolin-8-ol
DMF	*N*,*N*-dimethylformamide
DMPD	*N*,*N*-Dimethyl-*p*-phenylenediamine
DMSO	Dimethyl sulfoxide
DNA	Deoxyribonucleic acid
ECL	Enhanced chemiluminescence
ESI-MS	Electrospray ionization mass spectrometry
ESI-MS^2	Electrospray ionization tandom mass spectrometry
H_2O_2	Hydrogen peroxide
HBA	Hydrogen bond acceptor atoms
HBD	Hydrogen bond donor atoms
HEPES	4-(2-hydroxyethyl)-1-piperazineethanesulfonic acid
HRMS	High resolution mass spectrometer
K_d	Dissociation constant
logb	Stability constant
logBB	Calculated BBB partition coefficient
metal–Aβ	Metal-bound Aβ
MS	Mass spectrometry
MTT	3-(4,5-dimethyl-2-thiazolyl)-2,5-diphenyl-2*H*-tetrazolium bromide
MW	Molecular weight
NFTs	Neurofibrillary tangles
NMR	Nuclear magnetic resonance
$O_2^{\bullet-}$	Superoxide
PAMPA–BBB	Parallel artificial membrane permeability adapted for the blood–brain barrier

PBS	Phosphate buffered saline
pK_a	Acidity constant
PSA	Polar surface area
ptau	Phosphorylated tau
ROS	Reactive oxygen species
SDS	Sodium dodecyl sulfate
SPs	Senile plaques
TBS	Tris-buffered saline
TEM	Transmission Electron Microscopy
TLC	Thin Layer Chromatography
UV-vis	UV-visible spectroscopy

Chapter 1.

Pathological Features in Alzheimer's Disease and Chemical Tools to Understand Their Complexity

1.1 Introduction

Alzheimer's disease (AD), mortal neurodegenerative disease, is the most common form of dementia.[1] In 2016, over 33 million people worldwide were represented to be suffered from AD.[1] The number of patients is predicted to be about 131 million by 2050.[1] In AD brain, senile plaques (SPs) and neurofibrillary tangles (NFTs) which are composed by amyloid-β (Aβ) and phosphorylated tau (ptau) respectively, are considered as a hallmark of AD.[2-7] Including these hallmark, multiple pathological features (*i.e.*, Aβ aggregation, dishomeostesis and miscompartmentalization of metal ions, and oxidative stress) have been suggested to be independently or simultaneously affected in AD, causing the complexity of AD, the obstacle of illuminating its elemental cure of disease.[2,3,8-10]

The Aβ could aggregate themselves and form the SPs, the hallmark of AD.[9,11] In this senile plaques, metal ions [*i.e.*, Cu(I/II), Zn(II), and Fe(II/III)] is observed to be higher concentration than normal brain.[2,10,12-16] From redox-active metal ions [*i.e.*, Cu(I/II) and Fe(II/III)], reactive oxygen species (ROS) could be over produced by Fenton-like reaction.[2,10,12-15] Herein, we would be focusing on three hypothesis (*e.g.*, amyloid cascade hypothesis, metal ion hypothesis, and oxidative stress hypothesis) and their relationship and chemical tools to study them are described.

1.2 Alzheimer's Disease (AD)

1.2.1 Amyloid Cascade Hypothesis

The Aβ peptide is produced by proteolytic cleavage of the amyloid precursor protein (APP).[10,17] The β- and γ-secretases cleavage the transmembrane portion of the APP, and generate mainly two isoforms, $A\beta_{40}$ and $A\beta_{42}$.[2,3,8] The $A\beta_{42}$ have only two additional hydrophobic C-terminal residues (I41 and A42) which direct the peptide more aggregation; thus, $A\beta_{42}$ is considered more pathogenic than $A\beta_{40}$.[2-5,8]

After proteolytic cleavage, Aβ monomers interact with another monomer through their self-recognition site and initiate aggregation to larger species toward oligomers or fibrils.[2,3,8,9] Recently, among of these conformations, soluble Aβ oligomer is suggested more neurotoxic than other Aβ species through disrupting cellular membranes and signaling.[9,11]

1.2.2 Metal Ion Hypothesis

Homeostasis of metal ions is highly regulated in living organisms.[2,18] Cu and Zn are represented to be involved in neuronal transmission in the brain.[2,18-21] Therefore, broken of balance of metal ions can be a resulting in disease or death through initiate or develop the pathological pathway.[2,18] In the AD brain, SPs and NFTs are appeared with miscompartmentalization and dishomeostasis of metal ions.[2,6,22] In SPs of AD brain, highly concentration of Cu (*ca.* 0.4 mM), Zn (*ca.* 1 mM), and Fe (*ca.* 0.9 mM) have been detected.[2,6,13]

These high concentration of metal ions [*i.e.* Cu(I/II) and Zn(II)] could directly bind with Aβ and

forming the metal-associated Aβ (metal–Aβ) were observed.[2,10,12-15,23-25] Binding of Cu(II) to Aβ suggested to prefer a square planar geometry showing two coordination modes (component I and II) that are dependent on pH; Component I for pH 6.5 and Component II for pH 9).[6,14-16] In component I, Cu(II) is surrounded by a nitrogen (N) donor atom from N terminus, two N donor atoms from His residues (H6, and H13 or H14), and one oxygen (O) donor atom from backbone carbonyl group of D2 (3N1O).[2,6,13-15] Component II have 3N1O binding environment with one N donor atom from His residue (H6, H13, or H14), two N donor atom from N-terminus amine group and peptide backbone amine group of D1-A2, and one O donor atom from carbonyl group of A2-E3.[2,6,13-15] Zn(II) binding with Aβ is also expected to coordinate with four to six ligands; three His residues, an addition O donor atoms (D1, R5, Y10 or E11) and exogenous water molecule.[2,6,13-15]

1.2.3 Oxidative Stress Hypothesis

Redox active metal ions [*e.g.*, Cu(I/II) and Fe(II/III)] associated with Aβ are involved in Fenton-like reactions.[2,26] They are suggested to be implicated in producing pathway of the ROS [*e.g.*, Hydrogen peroxide (H_2O_2) and superoxide ($O_2^{\bullet-}$)] leading to oxidative stress. [2,4,26,27] When $O_2^{\bullet-}$ are produced too much to scavenged by superoxide dismutase, it could react with nitric oxide (NO) and form the peroxynitrite (ONO_2^-), which can oxidize the lipid, protein, and DNA.[3] Additionally, H_2O_2, strong oxidant, can react with organic molecules and form the peroxy adducts which could be implicated upregulate stress-activated protein kinases.[3]

1.3 Metal-bound Aβ and Chemical Tools in AD

1.3.1 Metal-bound Aβ

The metal ions [*e.g.*, Cu(II) and Zn(II)] associated Aβ are more facilitated aggregation pathway than metal-free Aβ and stabilize toxic soluble Aβ oligomer form.[2,13-16] Also, through the Fenton-like reaction, ROS could be overproduced in the brain.[2,10,12-15] For more understanding of metal–Aβ in AD, small molecule as a chemical tool was adopted to target and control the pathological pathway of metal–Aβ.

1.3.2 Design of Chemical Tools for Metal–Aβ

The small molecules for targeting the metal–Aβ, should have Aβ interaction moiety and metal binding site in the molecule.[5,25,28] For example, the dimethyl amino group is already known to be important in Aβ interaction when it is attached on the aromatic rings.[9,23,25,29-31] Furthermore, metal binding affinity of molecule is not in the appropriate range (*ca.* $K_d \sim 10^{-12}$–10^{-9} for Cu(II)–Aβ, $K_d \sim 10^{-9}$–10^{-6} for Zn(II)–Aβ), molecule could not interact with Aβ or just chelating out the metal ions from metal–

Aβ.[2,10] Additionally, for targeting the metal–Aβ in the brain, the molecules are preferred to be permeable toward blood-brain barrier (BBB) and water soluble.[25,32-34] The chemical tools to target metal–Aβ considered their Aβ interaction, metal binding and BBB permeability are determined their reactivity by *in vitro* assays.

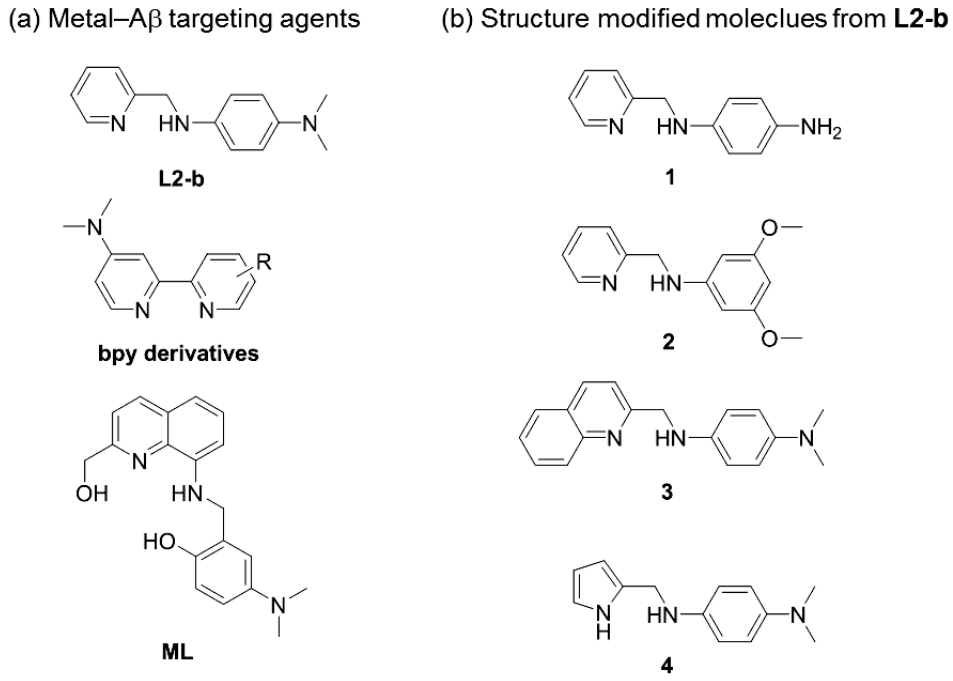

Figure 1.1. Library of chemical tools for targeting Metal–Aβ. (a) rationally designed small molecules (b) structure modified molecules from **L2-b**.

Following the incorporation design approach, the Aβ imaging agent, stilbene derivative was incorporated with metal binding donor atom.[5,25,28] The designed molecule (**L2-b**) have reactivity toward Cu(II)–Aβ and Zn(II)–Aβ; modulate the aggregation pathway of metal–Aβ over metal-free Aβ.[25] Furthermore, the structure of **L2-b** was employed to study the structure-activity relationship through the simple structure modification.[32] The simply modified molecule could target different pathological factors.[32] The modified molecules (**1**–**4**) could have different pathological factors for their target: **1** and **2** could target Cu(II)–Aβ; 3 could target both Cu(II)–Aβ and Zn (II)–Aβ; 4 could target all of metal-free Aβ, Cu(II)–Aβ and Zn (II)–Aβ.[32]

In contrast with **L2-b**, the molecules were designed from the metal chelator framework [*e.g.*, 2,2'-bipyridine (**bpy**)].[33] For interaction with Aβ, dimethyl amino group, which known as Aβ interaction moiety was incorporated on **bpy** backbone.[9,23,25,29-31] Also metal binding affinity was slightly modified by differently positioned methyl group.[33] These molecule also could modulate metal–Aβ aggregation pathway *in vitro*.[33]

In different design approach, coordination geometry (*e.g.*, square planar) of Cu(II) with ligand was fixed by molecular structure and prevented the reducing of Cu(II).[34] The designed molecule have 3N1O coordination environment with 8-hydroxyquinoline derivative.[34] Because of structure of molecule (**ML**), coordination with Cu(II) form the tilted square planar was designed which have tilted square planar when they bind with Cu(II).[34] Additionally, for Aβ interacting moiety was adopted to be reactive with Aβ.[34] Actually, **ML** could also modulate aggregation pathway of metal–Aβ, and suggested to decrease Cu(II) reducing toward Cu(I) by coordination geometry.[34]

The reactive molecules with metal–Aβ are investigated their neurotoxicity in the cell before *in vivo* experiments. From these studies, the knowledge of chemical tool design strategy and their reactivity could be valuable for another chemical tool or drug development.

1.4 Conclusions

AD is a critical disease for human being and more crucial in the future. Its complexity from multiple and inter-related pathological factors making the elucidation of etiology difficult. Currently the amyloid cascade hypothesis suggests that Aβ aggregates are involved in pathological pathway of AD. Additionally, metal ion dishomeostasis and miscompartmentalization is observed of another hallmark of AD. The metal ions [*e.g.*, Cu(II) and Zn(II)] binding Aβ and form metal–Aβ, facilitate the aggregation pathway, stabilize toxic oligomer form, and overproduce ROS resulting in oxidative stress. For better understanding of the role of metal–Aβ in AD, small molecules have developed as chemical tools to target metal–Aβ and modulate their pathological pathway. Several compounds with various frameworks have been employed to investigate the metal–Aβ interaction, and this study will be valuable to elucidate the unclear involvement of metal–Aβ in AD. Furthermore, the pharmacological properties of molecules will be helpful for designing different chemical tools or drug.

1.5 References

(1) Prince, M.; Comas-Herrera, A.; Knapp, M.; Guerchet, M.; Karagiannidou, M. *Workd Alzheimer Report 2016*; Alzheimer's Disease International: London, U.K., **2016**.

(2) Kepp, K. P. *Chem. Rev.* **2012**, *112*, 5193-5239.

(3) Jakob-Roetne, R.; Jacobsen, H. *Angew. Chem. Int. Ed.* **2009**, *48*, 3030-3059.

(4) Rauk, A. *Chem. Soc. Rev.* **2009**, *38*, 2698-2715.

(5) DeToma, A. S.; Salamekh, S.; Ramamoorthy, A.; Lim, M. H. *Chem. Soc. Rev.* **2012**, *41*, 608-621.

(6) Pithadia, A. S.; Lim, M. H. *Curr. Opin. in Chem. Biol.* **2012**, *16*, 67-73.

(7) Scott, L. E.; Orvig, C. *Chem. Rev.* **2009**, *109*, 4885-4910.

(8) Hamley, I. W. *Chem. Rev.* **2012**, *112*, 5147-5192.

(9) Lee, S. J. C.; Nam, E.; Lee, H. J.; Savelieff, M. G.; Lim, M. H. *Chem. Soc. Rev.* **2017**, *46*, 310-323.

(10) Savelieff, M. G.; Lee, S.; Liu, Y.; Lim, M. H. *ACS Chem. Biol.* **2013**, *8*, 856-865.

(11) Kotler, S. A.; Walsh, P.; Brender, J. R.; Ramamoorthy, A. *Chem. Soc. Rev.* **2014**, *43*, 6692-6700.

(12) Derrick, J. S.; Lim, M. H. *ChemBioChem* **2015**, *16*, 887-898.

(13) Faller, P.; Hureau, C. *Dalton Trans.* **2009**, 1080-1094.

(14) Faller, P. *ChemBioChem* **2009**, *10*, 2837-2845.

(15) Telpoukhovskaia, M. A.; Orvig, C. *Chem. Soc. Rev.* **2013**, *42*, 1836-1846.

(16) Tougu, V.; Tiiman, A.; Palumaa, P. *Metallomics* **2011**, *3*, 250-261.

(17) O'Brien, R. J.; Wong, P. C. *Annu. Rev. Neurosci.* **2011**, *34*, 185-204.

(18) Que, E. L.; Domaille, D. W.; Chang, C. J. *Chem. Rev.* **2008**, *108*, 1517-1549.

(19) Hung, Y. H.; Bush, A. I.; Cherny, R. A. *JBIC, J. Biol. Inorg. Chem.* **2010**, *15*, 61-76.

(20) Duce, J. A.; Bush, A. I. *Prog. Neurobiol.* **2010**, *92*, 1-18.

(21) Sensi, S. L.; Paoletti, P.; Bush, A. I.; Sekler, I. *Nat. Rev. Neurosci.* **2009**, *10*, 780.

(22) Bonda, D. J.; Lee, H.-g.; Blair, J. A.; Zhu, X.; Perry, G.; Smith, M. A. *Metallomics* **2011**, *3*, 267-270.

(23) Savelieff, M. G.; DeToma, A. S.; Derrick, J. S.; Lim, M. H. *Acc. Chem. Res.* **2014**, *47*, 2475-2482.

(24) Adlard, P. A.; Cherny, R. A.; Finkelstein, D. I.; Gautier, E.; Robb, E.; Cortes, M.; Volitakis, I.; Liu, X.; Smith, J. P.; Perez, K.; Laughton, K.; Li, Q.-X.; Charman, S. A.; Nicolazzo, J. A.; Wilkins, S.; Deleva, K.; Lynch, T.; Kok, G.; Ritchie, C. W.; Tanzi, R. E.; Cappai, R.; Masters, C. L.; Barnham, K. J.; Bush, A. I. *Neuron* **2008**, *59*, 43-55.

(25) Choi, J.-S.; Braymer, J. J.; Nanga, R. P. R.; Ramamoorthy, A.; Lim, M. H. *Proc. Natl. Acad. Sci. U. S. A.* **2010**, *107*, 21990-21995.

(26) Jomova, K.; Vondrakova, D.; Lawson, M.; Valko, M. *Mol. Cell. Biochem.* **2010**, *345*, 91-104.

(27) Eskici, G.; Axelsen, P. H. *Biochemistry* **2012**, *51*, 6289-6311.

(28) Rodríguez-Rodríguez, C.; Telpoukhovskaia, M.; Orvig, C. *Coord. Chem. Rev.* **2012**, *256*, 2308-2332.

(29) Derrick, J. S.; Kerr, R. A.; Korshavn, K. J.; McLane, M. J.; Kang, J.; Nam, E.; Ramamoorthy, A.; Ruotolo, B. T.; Lim, M. H. *Inorg. Chem.* **2016**, *55*, 5000-5013.

(30) Kung, H. F.; Lee, C.-W.; Zhuang, Z.-P.; Kung, M.-P.; Hou, C.; Plössl, K. *J. Am. Chem. Soc.* **2001**, *123*, 12740-12741.

(31) Kang, J.; Lee, S. J. C.; Nam, J. S.; Lee, H. J.; Kang, M.-G.; Korshavn, K. J.; Kim, H.-T.; Cho, J.; Ramamoorthy, A.; Rhee, H.-W.; Kwon, T.-H.; Lim, M. H. *Chem. Eur. J.* **2017**, *23*, 1645-1653.

(32) Beck, M. W.; Derrick, J. S.; Kerr, R. A.; Oh, S. B.; Cho, W. J.; Lee, S. J. C.; Ji, Y.; Han, J.; Tehrani, Z. A.; Suh, N.; Kim, S.; Larsen, S. D.; Kim, K. S.; Lee, J.-Y.; Ruotolo, B. T.; Lim, M. H. *Nat. Commun.* **2016**, *7*, 13115.

(33) Ji, Y.; Lee, H. J.; Kim, M.; Nam, G.; Lee, S. J. C.; Cho, J.; Park, C.-M.; Lim, M. H. *Inorg. Chem.* **2017**, *56*, 6695-6705.

(34) Lee, S.; Zheng, X.; Krishnamoorthy, J.; Savelieff, M. G.; Park, H. M.; Brender, J. R.; Kim, J. H.; Derrick, J. S.; Kochi, A.; Lee, H. J.; Kim, C.; Ramamoorthy, A.; Bowers, M. T.; Lim, M. H. *J. Am. Chem. Soc.* **2014**, *136*, 299-310.

Chapter 2.

Strategic Design of 2,2'-Bipyridine Derivatives to Modulate Metal−Amyloid-β Aggregation

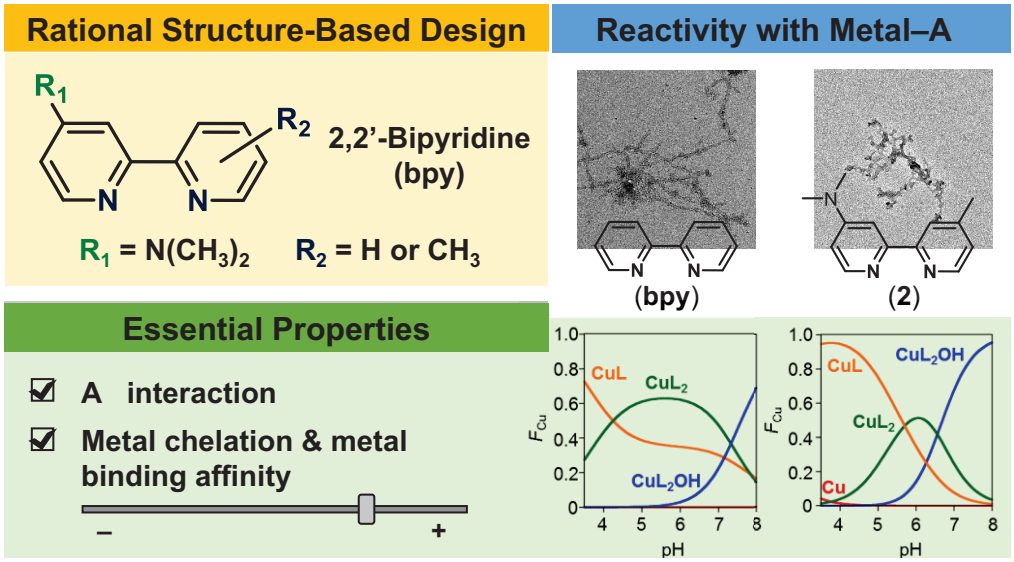

This chapter was adapted from the publication Ji, Y.; Lee, H. J.; Kim, M.; Nam, G.; Lee, S. J. C.; Cho, J.; Park, C. -M.; Lim, M. H. *Inorg. Chem.* **2017**, *56*, 6695-6705. I thank Professor Lim for her guidance and supporting throughout the writing of this article. I thank Dr. Hyuck Jin Lee for the studies of TEM, gel/Western blot, and cells; Dr. Shin Jung Lee for helping the analysis of mass spectrometric data.

2.1. Introduction

In 2016, over 47 million people worldwide were reported to be affected by dementia.[1] This number is speculated to reach about 131 million by 2050.[1] Alzheimer's disease (AD) is the most common form of dementia, representing 60 to 80% of cases.[1] Multiple pathological features [*e.g.*, amyloid-β (Aβ) aggregation, metal ions dyshomeostasis and miscompartmentalization, oxidative stress] have been observed to be individually or mutually involved in AD development, indicating the difficulty of elucidating its etiology.[2-8] Aβ peptides, one of the pathological factors, are denoted for their ability to self-aggregate and exist in various conformations, including monomers, oligomers, and fibrils.[2-5] Recently, among these conformations, Aβ oligomers have been suggested to be the toxic species able to damage cells through disrupting cellular membranes and signaling.[5,9] In addition, through the interaction between Aβ and membranes, Aβ aggregation is suggested to be facilitated resulting in the enhancement of its toxicity.[9] Moreover, abnormally high concentrations of metal ions [*ca.* 400 μM for copper and *ca.* 1 mM for zinc] are found from Aβ aggregates in the AD-affected brain.[4,6-8,10-16] These metal ions [*i.e.*, Cu(II) and Zn(II)] are reported to directly bind to Aβ, facilitate its aggregation, and promote the generation and stabilization of Aβ oligomers, suggested to be toxic.[4,6-8,10-16] Thus, metal-bound Aβ (metal–Aβ) complexes have been proposed to be linked to AD pathogenesis through direct interactions between metal ions and Aβ.[4,6-8,10-16]

To identify the relationship between metal–Aβ aggregation and neurotoxicity found in AD at the molecular level, chemical tools able to control the aggregation of metal–Aβ have been recently developed by rational structure-based design strategies.[7,12,17-28] Among them, some examples of small molecules have been constructed through the incorporation approach (*i.e.*, introduction of structural moieties critical for the desired properties, including metal binding and Aβ interaction, in a single molecular entity).[17,19,21,24,25,27,28] This design strategy has been producing such chemical tools with relatively small sizes [*e.g.*, molecular weight (MW) less than approximately 400 g/mol], giving them the advantage of being potentially available in the brain.[17] A recent study presented the smallest blood-brain barrier (BBB)-permeable chemical reagent, **DMPD** (MW = 136 g/mol), capable of interacting and reacting with both metal-free Aβ and metal–Aβ.[25]

Herein, we report a new class of compact 2,2'-bipyridine (**bpy**) derivatives (**1**–**4**; Figure 2.1) rationally designed to modulate the aggregation of metal–Aβ over metal-free Aβ. The bidentate ligand, **bpy** (structure shown in Figure 2.1), is commonly used as a metal chelator for various metal ions, including Cu(II) and Zn(II).[29-32] Until now, to the best of our knowledge, the **bpy** ligand itself as well as its derivatives have not been studied as potential chemical tools capable of interacting with complexes of metal–Aβ and altering their aggregation pathways. In order to control metal–Aβ aggregation, the essential properties of Aβ interaction and appropriate metal binding were instilled onto the **bpy** framework through two straightforward structural variations (Figure 2.1): (i)

incorporation of a reported Aβ targeting moiety, the dimethylamino functionality;[17,27,33-35] (ii) modification of metal binding affinities and/or steric hindrance at the metal chelation site *via* differently positioning an electron-donating methyl group[36] on the structure of **bpy**, along with a dimethylamino moiety,[36] thus changing the structural and electronic characteristics for metal binding. Our *in vitro* investigations, including metal binding, metal–Aβ interaction, and effects on metal-free Aβ and metal–Aβ aggregation, of the new **bpy** derivatives demonstrate that rational, straightforward structural variations on a simple metal chelator could construct novel chemical tools that can interact with metal–Aβ over metal-free Aβ, subsequently regulating metal–Aβ aggregation. Moreover, our structure-based design of compact compounds as modulators against metal–Aβ aggregation, presented in this work, could be further utilized to develop chemical tools for investigating metal–amyloid species found in amyloid-related disorders.

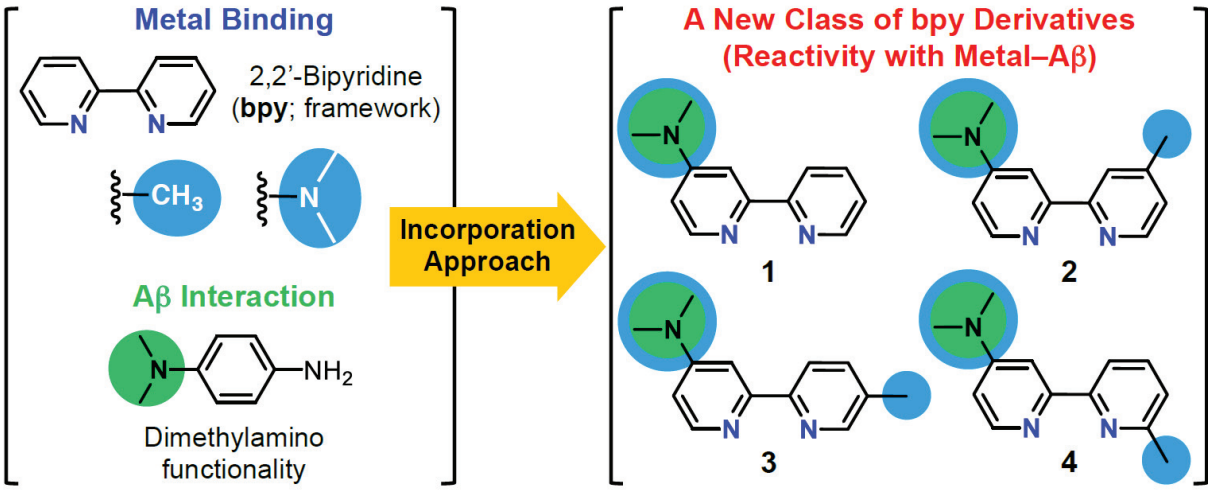

Figure 2.1. Rational structure-based design of chemical tools able to interact and react with metal–Aβ employing the framework of 2,2'-bipyridine (**bpy**). An Aβ interacting moiety (*i.e.*, dimethylamino functionality), along with a methyl group at different positions from the metal chelation site, was incorporated onto the **bpy** backbone. The N donor atoms for metal binding are highlighted in blue.

2.2. Results and Discussion

2.2.1. Design Rationale and Preparation of bpy Derivatives.

Through the incorporation approach, a new class of small molecules (**bpy** derivatives; Figure 2.1) was designed by installing a dimethylamino group (for Aβ interaction and electronic influence on metal binding)[17,27,33-36] as well as a methyl group (for electron donation and/or steric hindrance)[30,36,37] onto the **bpy** framework. A well-known metal chelator, **bpy** (Figure 2.1), was selected as the main structural backbone based on multiple characteristics: (i) the capability of binding to metal ions through two nitrogen (N) donor atoms [particularly, Cu(II) and Zn(II); formation constant values

(logk_f) of Cu(II)–**bpy** and Zn(II)–**bpy** have been reported to be *ca.* 7.0 and *ca.* 6.0, respectively][29-32]; (ii) relatively good solubility in aqueous media (*e.g.*, 5.9 mg/mL in water)[38]; (iii) potential applications in the brain (*e.g.*, intraperitoneally administered **bpy** was able to prevent and reduce intracerebral hemorrhage *in vivo*)[39]; (iv) ease of structural transformations.[40] In addition, previous studies of **bpy** reported its ability to regulate metal-mediated reactions in biological systems [*e.g.*, reducing the formation of hydrogen peroxide triggered by Fe(II/III)],[41,42] supporting its applicability in biology.

The new **bpy** derivatives (**1**–**4**; Figure 2.1) were fashioned to change their binding affinities to Cu(II) and Zn(II). Such variation in the metal binding affinities of the **bpy** derivatives was achieved by introducing a dimethylamino group on one pyridine ring as well as a methyl group as an electron-donating group[36] at *ortho*, *meta*, and *para* positions to the N atom on the other pyridine ring. In addition to the electronic aspect, the incorporation of a methyl group at the *ortho* position to the N donor atom of the pyridine ring (**4**, Figure 2.1) was expected to exhibit steric hindrance at the metal chelation site, as previously presented.[30,37] Moreover, to introduce Aβ interaction onto the backbone of **bpy**, the dimethylamino functionality, suggested to be an Aβ interacting portion,[17,27,33-35] was located at the *para* position to the N donor atom of one pyridine ring where the steric interference between its metal chelation site and the Aβ interacting group could be minimized (see **1**–**4**).

Scheme 2.1. Synthetic routes to **1**–**4**.

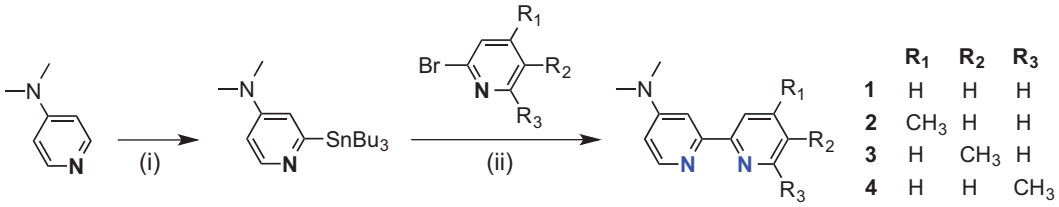

	R_1	R_2	R_3
1	H	H	H
2	CH_3	H	H
3	H	CH_3	H
4	H	H	CH_3

Reagents and conditions: (i) *n*-BuLi, 2-dimethylaminoethanol, hexanes, 0 °C; Bu_3SnCl, –78 °C, yield: 78%; (ii) $PdCl_2(PPh_3)_2$, LiCl, PPh_3, toluene, 110 °C, yield (for **1**–**4**): 33-50%.

The new **bpy** derivatives (**1**–**4**) were synthesized as depicted in Scheme 1. The precursor, *N,N*-dimethyl-2-(tributylstannyl)pyridin-4-amine, was produced by stannylation of lithiated 4-dimethylaminopyridine with tributyltin chloride. The **bpy** derivatives were prepared by a Stille cross-coupling reaction,[43,44] in which *N,N*-dimethyl-2-(tributyl-stannyl)pyridin-4-amine was allowed to react with the appropriate aryl bromides (2-bromopyridine or 2-bromo-*n*-methylpyridine, *n* = 4-6) using the palladium catalyst, $PdCl_2(PPh_3)_2$ (5 mol%), and triphenylphosphine. All **bpy** derivatives were obtained through purification by column chromatography in modest yields (*ca.* 33-50%).

2.2.2. Metal Binding Properties of bpy Derivatives.

First, metal binding of the newly prepared **bpy** derivatives (**1**–**4**; Figure 2.1) was monitored by UV–

visible spectroscopy (UV−vis) (Figure 2.2). The **bpy** ligand showed spectral changes upon addition of Cu(II) and Zn(II), consistent with previously reported data.[31,32] Two noticeable alterations in the UV−vis spectra of the **bpy** derivatives in the presence of $CuCl_2$ were observed (Figure 2.2a): (i) hyperchromic shifts at *ca.* 300/310 nm (for **bpy**) or *ca.* 340 nm (for **1**–**4**); (ii) bathochromic shifts of the overall spectra. The samples coincubated with the **bpy** derivatives and $ZnCl_2$ exhibited similar optical changes to those treated with $CuCl_2$ with the exception of **4** (Figure 2.2b), displaying hyperchromic shifts of the peaks at *ca.* 295/306 nm (for **bpy**) or *ca.* 248/282 nm (for **1**–**4**) accompanied by a relatively less significant bathochromic shift of the overall spectra. Binding of the **bpy** derivatives with Cu(II) or Zn(II) was evidenced by these optical deviations.

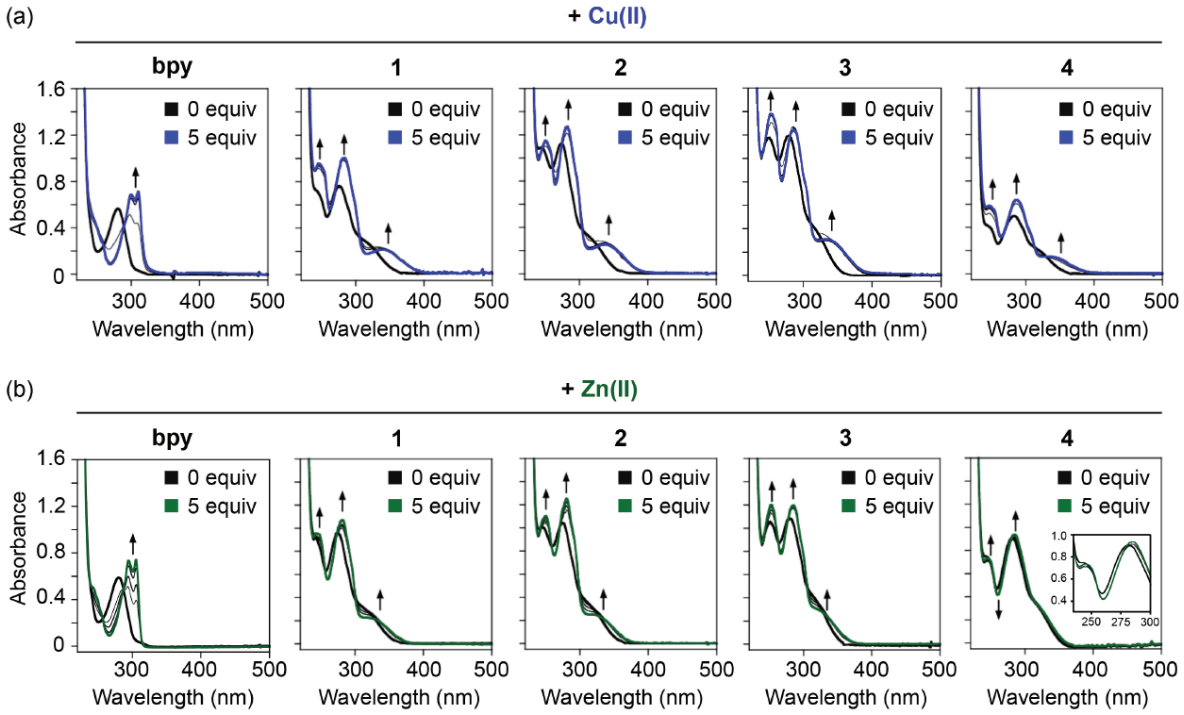

Figure 2.2. Cu(II) and Zn(II) binding of **bpy** and **1**–**4**. UV−vis spectra of ligands (black lines) upon addition of Cu(II) or Zn(II) (from 0.5 to 5 equiv). Conditions: [compound] = 50 μM [for **bpy** and **1**–**3**; [**4**] = 50 μM (for Cu(II) binding) and 100 μM (for Zn(II) binding)]; [$CuCl_2$ or $ZnCl_2$] = 0, 25, 50, 100, and 250 μM (for **1**–**3**; for **4**, [$CuCl_2$] = 0, 25, 50, 100, and 250 μM, [$ZnCl_2$] = 0, 50, 100, 200, and 500 μM); pH 7.4; 10 min; room temperature.

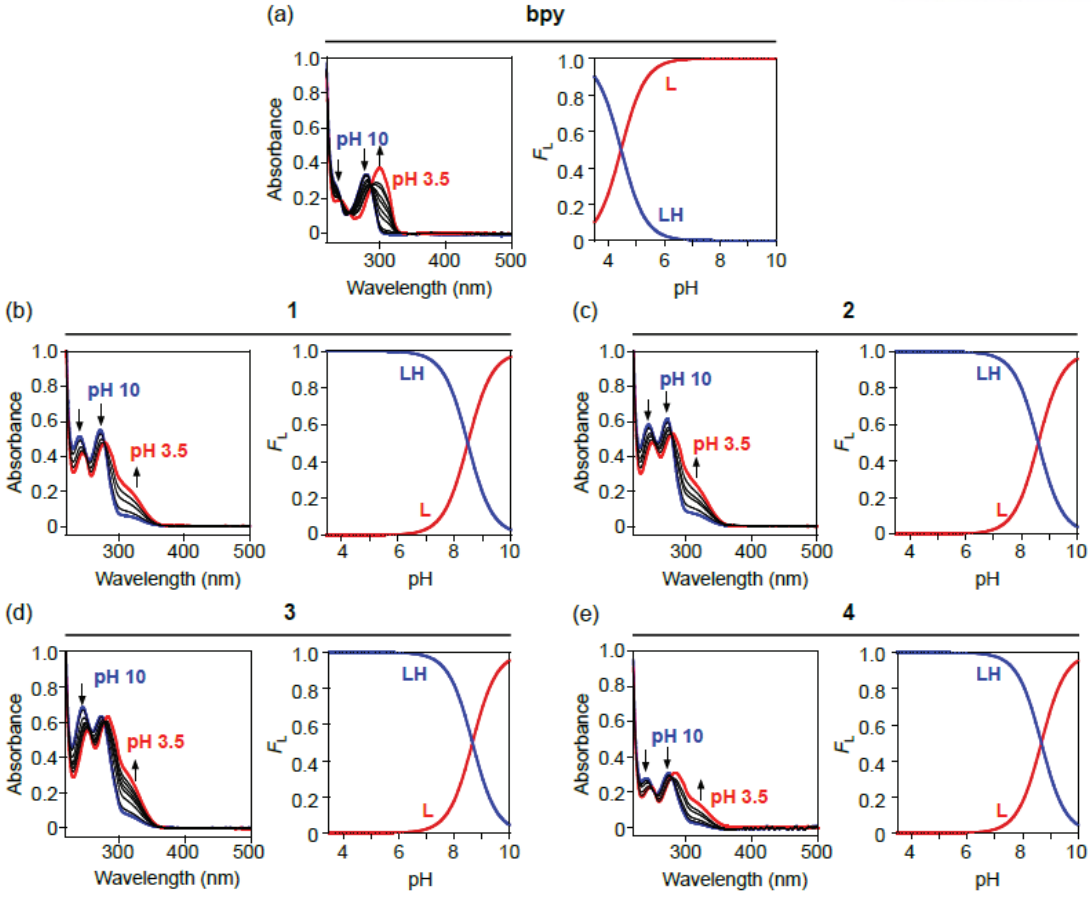

							pK_a[a]					
						L =	**bpy**	**1**	**2**	**3**	**4**	
LH	⇌	L	+	H	(pK_{a1})		4.46(0)	8.47(8)	8.59(3)	8.66(6)	8.67(4)	

Figure 2.3. Solution speciation studies of **bpy** and **1**–**4**. UV−vis variable-pH titration spectra (left) and solution speciation diagrams (right) of (a) **bpy**, (b) **1**, (c) **2**, (d) **3**, and (e) **4** (F_L = fraction of species at given pH). Acidity constants (pK_as) of L (L = **bpy** and **1**–**4**) are summarized in the table (bottom). Conditions: [L] = 25 μM; room temperature. Charges are omitted for clarity. [a]The error in the last digit is shown in the parentheses.

Second, UV−vis variable-pH titration experiments were conducted to determine the solution speciation of the **bpy** derivatives in the absence and presence of Cu(II) or Zn(II) (Figure 2.3, 2.4, and 2.5). Based on the titration results of **bpy** and **1**–**4**, the solution speciation diagrams were depicted in Figure 2.3. The diagrams (i) revealed that two solution species of **bpy** and **1**–**4** [*i.e.*, neutral (L) and monoprotonated (LH) forms (protonated at the N atom on the pyridine ring with the dimethylamino functionality)] existed in the pH range of *ca.* 3.5-6 for **bpy** and *ca.* 6-10 for **1**–**4**; (ii) predicted L and LH to be the predominant species for **bpy** and **1**–**4**, respectively, at a physiological pH (*i.e.*, 7.4); (iii) determined the acidity constants (pK_as) of the ligands [for **bpy**, pK_a = 4.46(0); for **1**, pK_a = 8.47(8); for **2**, pK_a = 8.59(3); for **3**, pK_a = 8.66(6); for **4**, pK_a = 8.67(4)]. The electron density of the N atom was enhanced from the electron donation of the dimethylamino group,[36] incorporated at the *para* position

to N donor atom of one pyridine ring, resulting in the elevation of the **bpy** derivatives' pK_a values. Protonation at the N atom of **1**–**4** was estimated to be relatively easier than that of **bpy**. Thus, the structural variation which could lead to the modified pK_a values of the N donor atom(s), responsible for metal binding, could alter metal binding affinities of molecules and subsequently direct their ability to modulate metal–Aβ aggregation (*vide infra*). Additionally, the introduction of a methyl group on the **bpy** framework also raised the pK_a.

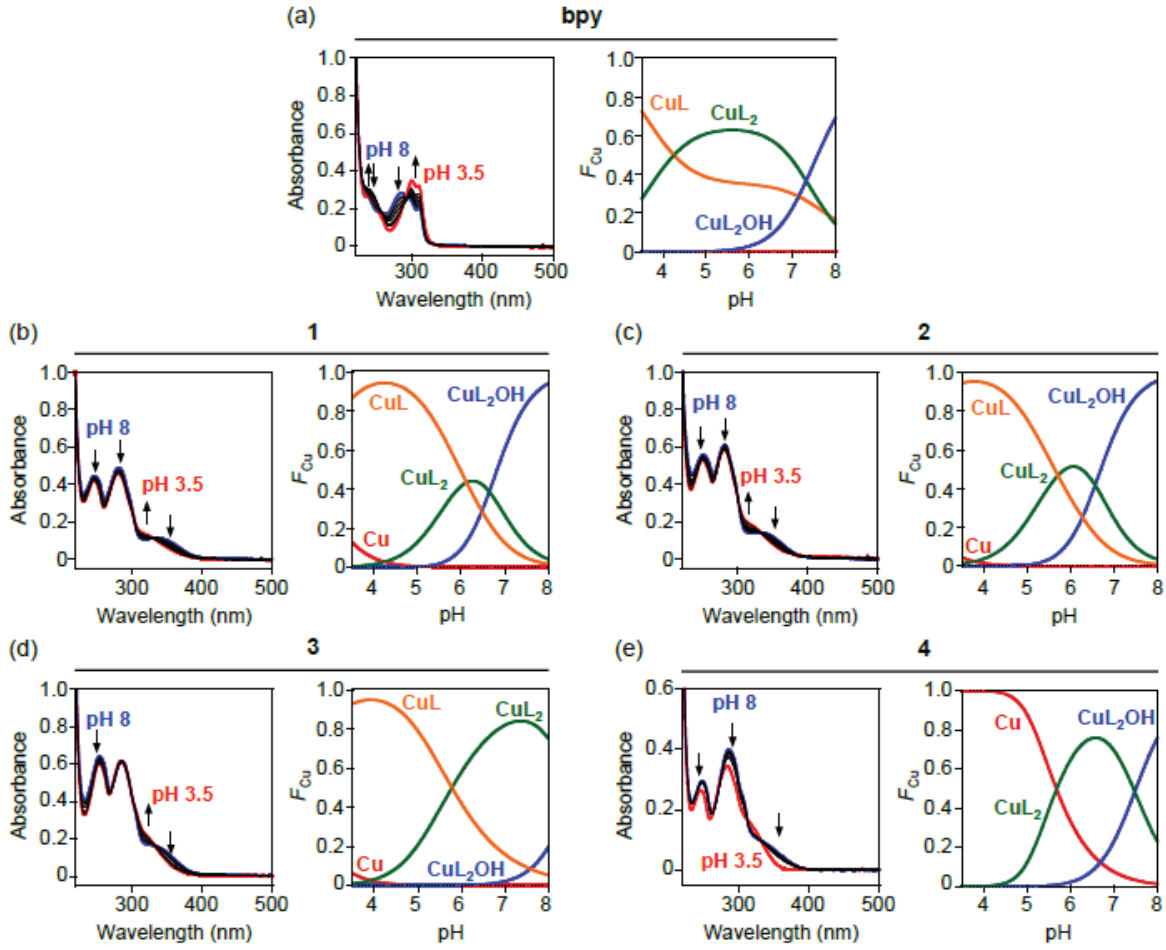

		logβ^a				
	L =	**bpy**	**1**	**2**	**3**	**4**
Cu + 2L + OH ⇌	$Cu(L)_2(OH)$	8.64(6)	11.63(7)	12.90(7)	10.73(1)	8.32(0)
Cu + 2L ⇌	$Cu(L)_2$	15.96(7)	18.28(3)	19.46(9)	19.31(1)	15.79(9)
Cu + L ⇌	Cu(L)	10.34(4)	10.66(3)	11.34(4)	11.22(8)	12.96(1)
pCu (= -log[$Cu_{unchelated}$]; pH 6.6 / 7.4)		10.34 / 10.34	8.80 / 9.54	9.37 / 10.12	9.17 / 9.92	5.77 / 6.32

Figure 2.4. Solution speciation studies of Cu(II)–L complexes (L = **bpy** and **1**–**4**). UV−vis variable-pH titration spectra (left) and solution speciation diagrams (right) of (a) **bpy**, (b) **1**, (c) **2**, (d) **3**, and (e) **4** upon incubation with Cu(II) (F_{Cu} = fraction of species at given pH). Stability constants (logβ) of Cu(II)–L complexes are summarized in the table (bottom). Charges are omitted for clarity. Conditions: [L] = 25 μM; [$CuCl_2$] = 12.5 μM; room temperature. [a]The error in the last digit is shown in the parentheses.

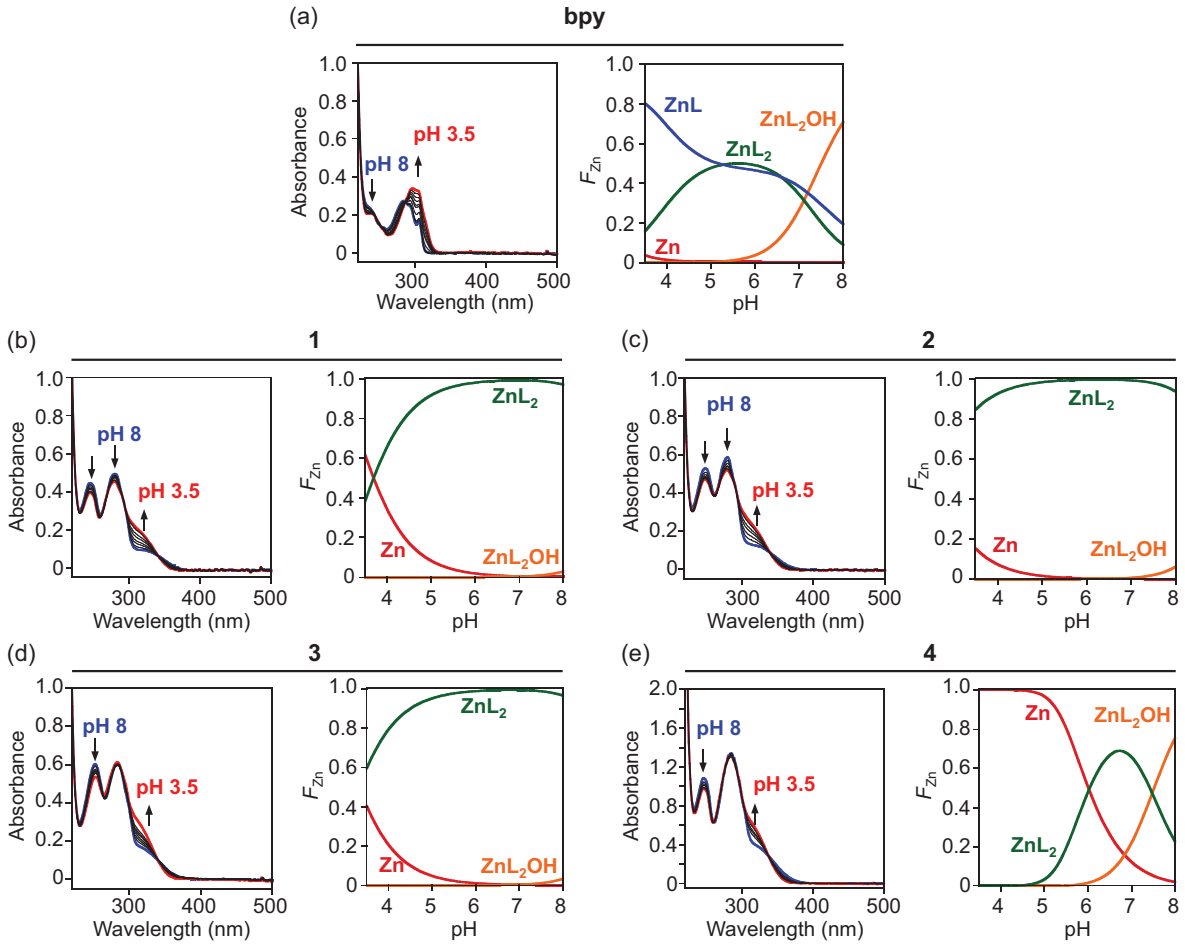

			log [a]				
		L =	**bpy**	**1**	**2**	**3**	**4**
Zn + 2L + OH	⇌	$Zn(L)_2(OH)$	5.45(4)	9.83(9)	12.57(9)	11.02(0)	6.43(9)
Zn + 2L	⇌	$Zn(L)_2$	12.56(0)	19.37(4)	21.76(0)	20.49(1)	13.91(5)
Zn + L	⇌	Zn(L)	7.29(6)	—	—	—	—
pZn (= -log[$Zn_{unchelated}$]; pH 6.6 / 7.4)			7.30 / 7.31	7.05 / 7.55	7.77 / 8.27	7.30 / 7.80	4.96 / 5.50

Figure 2.5. Solution speciation studies of Zn(II)–L complexes (L = **bpy** and **1**–**4**). UV–vis variable-pH titration spectra (left) and solution speciation diagrams (right) of (a) **bpy**, (b) **1**, (c) **2**, (d) **3**, and (e) **4** upon incubation with Zn(II) (F_{Zn} = fraction of species at given pH). Stability constants (logβ) of Zn(II)–L complexes are summarized in the table (bottom). Charges are omitted for clarity. Conditions: [L] = 25 μM (for **bpy** and **1**–**3**) or 100 μM (for **4**); [$ZnCl_2$] = 12.5 μM (for **bpy** and **1**–**3**) or 50 μM (for **4**); room temperature. [a]The error in the last digit is shown in the parentheses.

Once the pK_a values of the ligands were determined, the solution speciation experiments of Cu(II)–/Zn(II)–ligand complexes were carried out in a pH range of 3.5-8. The dissociation constants ($K_d \approx [Cu_{unchelated}]$ or $[Zn_{unchelated}]$; pCu = $-\log[Cu_{unchelated}]$; pZn = $-\log[Zn_{unchelated}]$) of Cu(II) or Zn(II) complexes with the **bpy** derivatives were identified based on the stability constants (logβ) and the pCu and pZn values (Figures 2.4 and 2.5). In the pH range, the speciation studies of Cu(II) and Zn(II)

complexes with **bpy** and **1**–**4** indicated the presence of Cu(II)– or Zn(II)–ligand complexes with the 1:1 and/or 1:2 metal-to-ligand stoichiometry at pH 7.4 (Figures 2.4 and 2.5). As for the metal binding affinities of the **bpy** derivatives at a physiological pH (*i.e.*, 7.4), **1**–**3** were observed to have binding affinities to Cu(II) and Zn(II) in the nanomolar and low micromolar range, respectively, except for **4** (micromolar and high micromolar for Cu(II) and Zn(II), respectively). The metal binding affinities of **bpy** derivatives were determined to be altered due to the changed electron density on the N donor atoms, responsible for metal chelation, by the incorporation of the dimethylamino and/or methyl group(s). In addition, in both Cu(II)- and Zn(II)-containing experimental sets, **4**, containing a methyl group located at the *ortho* position to the N donor atom on a pyridine ring (steric hindrance), exhibited the weakest binding affinities for both metal ions, compared to the other derivatives (**1**–**3**), as expected. Collecting these results, the methyl substituent's position on the **bpy** framework, along with installation of a dimethylamino group, is a factor in varying the binding affinities of the **bpy** derivatives to Cu(II) and Zn(II). Overall, the K_d values of Cu(II)– and Zn(II)–ligand (*i.e.*, **bpy** and **1**–**3**) complexes were within the appropriate range for interaction with metal ions surrounded by Aβ [K_d, *ca.* 10^{-12}–10^{-9} M for Cu(II)–Aβ; K_d, *ca.* 10^{-9}–10^{-6} M for Zn(II)–Aβ],[4,6,10,11] while those of **4** were not within this range, suggesting that **bpy** and **1**–**3** could affect metal–Aβ aggregation pathways (*vide infra*).

2.2.3. Interactions of bpy Derivatives with Metal-free Aβ and Metal–Aβ.

Electrospray ionization mass spectrometry (ESI-MS) was employed to investigate how the **bpy** derivatives interact with Aβ in the absence and presence of Cu(II). Note that Zn(II)–Aβ complexes were not detectable under our MS conditions. As shown in Figure 2.6a, upon incubation of **bpy**, **1**, and **4** with metal-free $Aβ_{40}$, the MS spectra did not indicate compound–Aβ interactions, such as Aβ–ligand adduct formation and peptide modifications (*i.e.*, oxidation, cleavage), suggested mechanisms for modulating Aβ aggregation.[21,25,27,28,34,35]

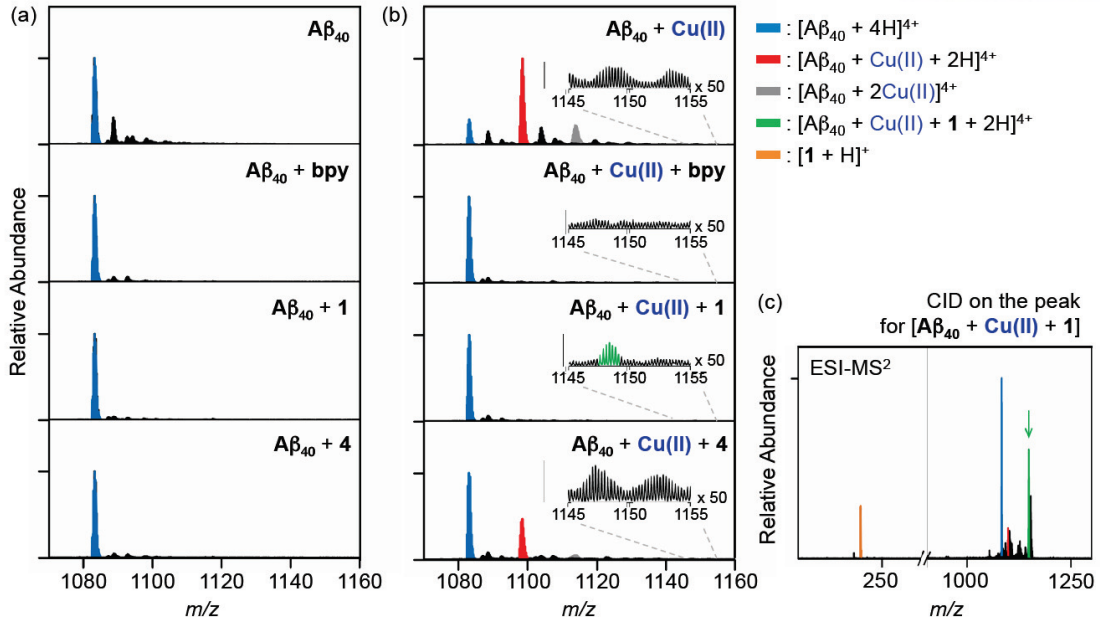

Figure 2.6. ESI-MS spectra of $A\beta_{40}$ incubated with excess amounts of compounds (**bpy**, **1**, and **4**) in the absence and presence of Cu(II). ESI-MS spectra of $A\beta_{40}$ without (a) and with (b) Cu(II). Conditions: $[A\beta_{40}]$ = 100 μM; $[CuCl_2]$ = 100 μM; [compound] = 500 μM; 20 mM ammonium acetate, pH 7.2 (1% v/v DMSO); 37 °C; 1 h incubation; no agitation; 10-fold diluted samples were injected to the mass spectrometer. (c) Tandem MS (ESI-MS^2) spectrum of the +4-charged ternary complex ($[A\beta_{40}$ + Cu(II) + **1** + $2H]^{4+}$, 1148 *m/z*). The ESI-MS^2 results support the formation of a ternary complex composed of $A\beta_{40}$, Cu(II), and **1**. The relative abundance of each spectrum was individually normalized based on the highest peak.

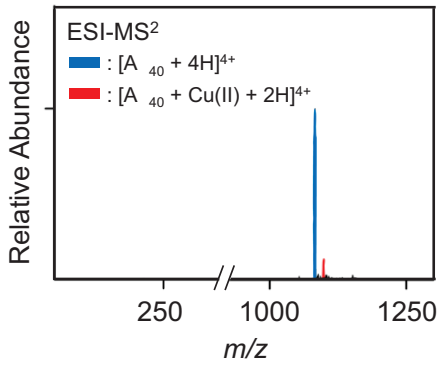

Figure 2.7. Tandem MS (ESI-MS^2) spectrum of the +4-charged peak at 1151 *m/z* from the sample containing $A\beta_{40}$, Cu(II), and **4**. The ESI-MS^2 results supported that the peak was assigned to $[A\beta + 2Cu + 2K + 4H_2O - 2H]^{4+}$, thus indicating no formation of a ternary complex composed of $A\beta_{40}$, Cu(II), and **4**. Conditions: $[A\beta_{40}]$ = 100 μM; $[CuCl_2]$ = 100 μM; [compound] = 500 μM; 20 mM ammonium acetate, pH 7.2 (1% v/v DMSO); 37 °C; 1 h incubation; no agitation; the 10-fold diluted samples were injected to the mass spectrometer. The relative abundance of each spectrum was individually normalized based on the highest peak.

As depicted in Figure 2.6b, a noticeable decrease in the relative abundance of Cu(II)–$A\beta_{40}$ (assigned as red peaks) in the ESI-MS spectra was monitored when Cu(II)–$A\beta_{40}$ samples were treated with **bpy**, **1**, or **4**. The observed reduction in the signal of Cu(II)–$A\beta_{40}$ may be accounted for by two possible explanations: (i) **bpy**, **1**, and **4** may accelerate the Cu(II)–Aβ aggregation, thus significantly decreasing the amount of monomeric Cu(II)–Aβ present in solution; (ii) **bpy**, **1**, and **4** may sequester Cu(II) from Cu(II)–Aβ potentially altering metal–Aβ aggregation pathways. Additionally, the production of a ternary complex [*i.e.*, Cu(II)–$A\beta_{40}$–**1**, 1148 *m/z*] was verified by ESI-MS from Cu(II)–$A\beta_{40}$ samples treated with **1** (Figure 2.6b; green peak). The tandem MS (ESI-MS^2) analysis of the ternary complex indicated the peaks denoting ions of Cu(II)–$A\beta_{40}$, metal-free $A\beta_{40}$, and **1** (Figure 2.6c). Based on the detection of the Cu(II)–$A\beta_{40}$–**1** complex, the incorporation of the dimethylamino functionality seems to markedly promote the interaction between the ligand and metal–Aβ as expected. Furthermore, based on previously reported studies,[21,24,28] the generation of a ternary complex composed of **1** and Cu(II)–Aβ proposes its capability of modifying metal–Aβ aggregation pathways (*vide infra*). In contrast, as depicted in Figure 2.6b, the presence of the remaining Cu(II)–$A\beta_{40}$ peak was detected in the sample of Cu(II)–$A\beta_{40}$ treated with **4**. The expected *m/z* value (1151 *m/z*) for a ternary complex composed of Cu(II)–$A\beta_{40}$ and **4** was observed by ESI-MS (Figure 2.6b); however, our ESI-MS^2 analysis indicated that the peak contained $A\beta_{40}$ and Cu(II) without **4** (Figure 2.7), thus being assigned as $[A\beta_{40} + 2Cu + 2K + 4H_2O - 2H]^{4+}$ (no generation of a ternary complex between metal–Aβ and **4**). Overall, these different interactions of **1** and **4** with Aβ in the presence of Cu(II) could be correlated with their metal binding affinities affecting their ability to bind to Cu(II) surrounded by Aβ (*vide supra*). Taken together, the ESI-MS and ESI-MS^2 studies suggest that the introduction of the dimethylamino functionality onto the **bpy** backbone could enhance the molecule's interaction with Cu(II)–Aβ. Additionally, the varied metal binding properties of the **bpy** derivatives through the inclusion of a methyl group on the framework were shown to be related to their ability to interact with Cu(II)–Aβ. Such differentiated degrees of interaction between the **bpy** derivatives and Cu(II)–Aβ, along with no apparent interaction with metal-free Aβ, could be a corresponding feature directing their controlling reactivity towards metal–Aβ aggregation over metal-free Aβ analog (*vide infra*).

2.2.4. Effects of bpy Derivatives on Aggregation of Metal-free Aβ and Metal–Aβ.

In order to identify the ability of the **bpy** derivatives to regulate Aβ aggregation in both the absence and presence of metal ions [*i.e.*, Cu(II) and Zn(II)], experiments able to indicate their influence on the formation of Aβ aggregates upon treatment with compounds were performed (Figure 2.8a). We employed gel electrophoresis with Western blotting (gel/Western blot) utilizing an anti-Aβ antibody

(6E10) and transmission electron microscopy (TEM) to analyze the MW distributions and morphological changes of the resultant Aβ species upon incubation with the **bpy** derivatives, respectively (Figures 2.8 and 2.9). Under our experimental conditions, compound-free Aβ samples with and without metal ions are generally observed to produce aggregates with high MWs (*e.g.*, fibrils) that are too bulky to penetrate the gel matrix, yielding a small amount of smearing in the gels.[27,28,34,35] These large-sized Aβ aggregates were visualized *via* TEM.[27,28,34,35]

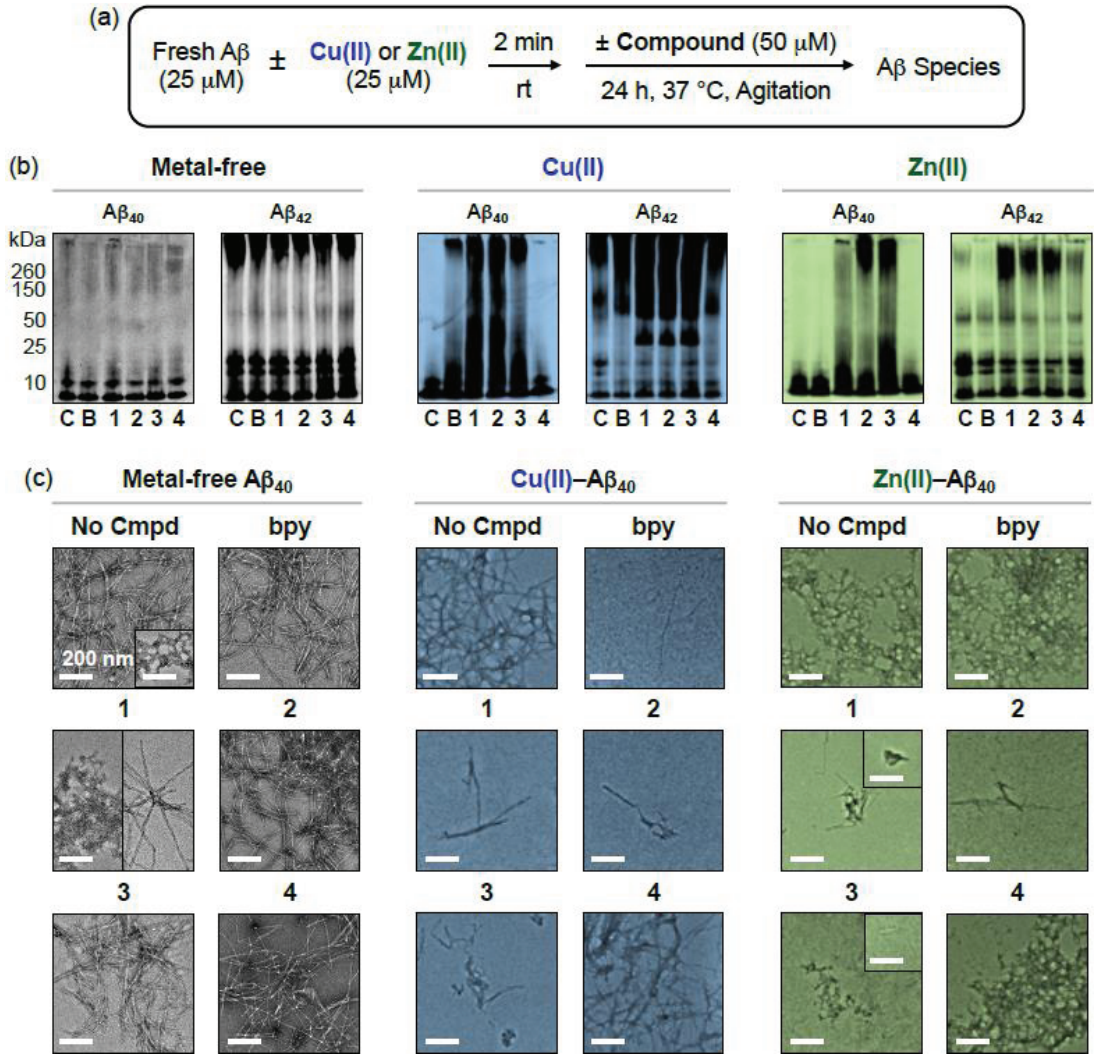

Figure 2.8. Effects of **bpy** and **1**–**4** towards formation of metal-free Aβ and metal–Aβ aggregates. (a) Scheme of the experiments. (b) Visualization of the resultant $Aβ_{40}$ and $Aβ_{42}$ species by gel electrophoresis with Western blotting (gel/Western blot) using an anti-Aβ antibody (6E10). Conditions: [Aβ] = 25 μM; [$CuCl_2$ or $ZnCl_2$] = 25 μM; [compounds] = 50 μM; 24 h; pH 6.6 (for Cu(II)-treated experiments) or pH 7.4 (for metal-free and Zn(II)-added experiments); 37 °C; constant agitation. Lanes: (**C**) [Aβ (± $CuCl_2$ or $ZnCl_2$)]; (**B**) [(C) + **bpy**]; (**1**) [(C) + **1**]; (**2**) [(C) + **2**]; (**3**) [(C) + **3**]; (**4**) [(C) + **4**]. (c) TEM images of the 24 h incubated $Aβ_{40}$ samples from (b) [the TEM images of the resultant $Aβ_{42}$ aggregates from (b) are presented in Figure 2.9]. The insets represent the minor species. Scale bar = 200 nm.

As shown in Figure 2.8b (left column), the gel/Western blot results demonstrated that **bpy** and its derivatives did not exhibit any reactivity against both $A\beta_{40}$ and $A\beta_{42}$ in the absence of metal ions. The MW distributions of Cu(II)–$A\beta_{40}$/$A\beta_{42}$ species, but not Zn(II)–$A\beta_{40}$/$A\beta_{42}$ species, were altered with the treatment of **bpy** (Figure 2.8b, middle and right columns, lane B). On the other hand, the compounds embodying the dimethylamino functionality (*i.e.*, **1**–**3**; except for **4**) were able to noticeably vary the sizes of both Cu(II)–$A\beta_{40}$/$A\beta_{42}$ species and Zn(II)–$A\beta_{40}$/$A\beta_{42}$ species to different extents, indicating the generation of a mixture of peptide species with various MWs (Figure 2.8b, middle and right columns, lanes 1-3). As expected from the studies of metal binding and metal–Aβ interaction (*vide supra*), **4** did not show its perceivable activity in modulation of both Cu(II)–$A\beta_{40}$/$A\beta_{42}$ and Zn(II)–$A\beta_{40}$/$A\beta_{42}$ aggregation (Figure 2.8b, middle and right columns, lane 4).

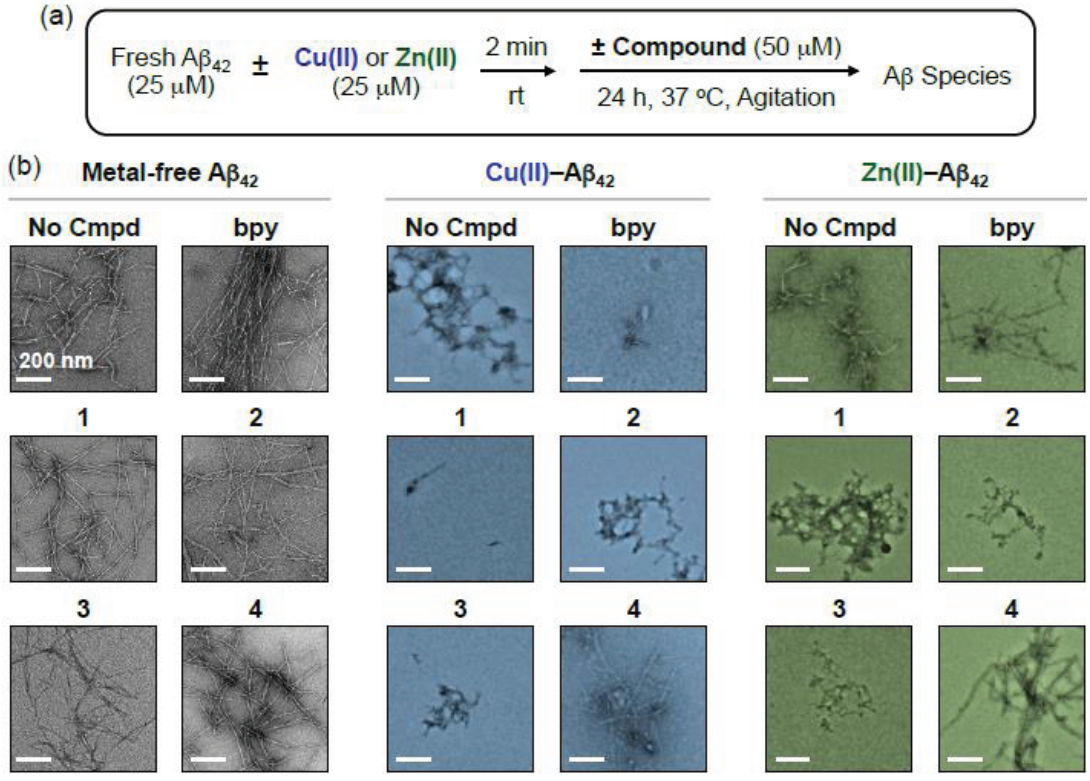

Figure 2.9. TEM images of the resultant metal-free $A\beta_{42}$ and metal–$A\beta_{42}$ aggregates generated upon treatment with **bpy** and **1**–**4**. (a) Scheme of the experiments. (b) TEM images of the 24 h incubated $A\beta_{42}$ samples from Figure 2.8. Scale bar = 200 nm.

In addition to the gel/Western blot, the morphologies of both resultant $A\beta_{40}$ and $A\beta_{42}$ aggregates upon addition of **bpy** and **1**–**4** were analyzed by TEM. As presented in Figures 2.8c and 2.9b (left column), metal-free Aβ aggregates produced by incubation with **bpy** or **1**–**4** were shown to have similar morphologies to those generated under compound-free conditions. Different from metal-free

conditions, Cu(II)–Aβ samples treated with **bpy** demonstrated smaller unstructured aggregates, but no significant morphological variation of the **bpy**-treated Zn(II)–Aβ aggregates was revealed (Figures 2.8c and 2.9b, middle and right columns). In both Cu(II)–Aβ and Zn(II)–Aβ samples containing **1**–**3**, peptide aggregates with distinctive morphologies (*i.e.*, thinner/shorter fibers and amorphous species), compared to those from compound-free metal–Aβ samples, were exhibited (Figures 2.8c and 2.9b, middle and right columns). On the contrary, **4** could not affect the morphologies of the resultant Aβ aggregates under metal-treated conditions (Figures 2.8c and 2.9b), as expected from its lack of interaction with metal–Aβ and modulation of metal–Aβ aggregation, demonstrated by the ESI-MS and gel/Western blot experiments, respectively (Figures 2.6b and 2.8b).

Based on the overall observations, both the dimethylamino and methyl groups are indicated to alter the compounds' ability to control the aggregation pathways of metal-treated $A\beta_{40}$ and $A\beta_{42}$. To be more specific, the **bpy** derivatives (**1**–**3**) containing a dimethylamino moiety with proper metal binding affinities were shown to have their regulatory reactivity against Aβ aggregation in the presence of Cu(II) and Zn(II). Although **4**'s structure includes the dimethylamino functionality (like **1**–**3**), the methyl group at the *ortho* position to the N donor atom of a pyridine ring appears to change its metal binding affinities thus hampering the compound's capacity to impact metal–Aβ aggregation pathways.

2.2.5. Biological Properties of bpy Derivatives.

In addition to their *in vitro* reactivity towards metal–Aβ, the potential of our **bpy** derivatives to be used in biological systems was investigated. For potent applications in brain, BBB permeability of the **bpy** derivatives was analyzed. As summarized in Table 1, based on Lipinski's rules, calculated logBB values (logBB = logarithm of the ratio between the concentration of a drug in the brain and that in the blood), and the $-\log P_e$ values measured by the *in vitro* parallel artificial membrane permeability assay adapted for the BBB (PAMPA–BBB),[45-47] the **bpy** derivatives were suggested to be BBB permeable.

Table 2.1. Values (MW, *c*log*P*, HBA, HBD, PSA, logBB, and $-\log P_e$)[a] for **bpy** and **1**–**4**.

Compounds	MW	*c*log*P*	HBA	HBD	PSA (Å^2)	logBB	logP_e	CNS± prediction
bpy	156	1.56	2	0	25.8	−0.0140	4.45 (± 0.13)	CNS+
1	199	2.32	3	0	27.0	0.0820	4.51 (± 0.01)	CNS+
2	213	2.82	3	0	29.1	0.128	4.45 (± 0.01)	CNS+
3	213	2.82	3	0	29.1	0.128	4.43 (± 0.01)	CNS+
4	213	2.82	3	0	29.1	0.128	4.51 (± 0.01)	CNS+
Lipinski's rules and others	≤ 450	≤ 5.0	≤ 10	≤ 5	≤ 90	<−1.0 (poorly distributed in the brain)	< 5.4; > 5.7	CNS+; CNS−

[a]MW, molecular weight; *c*log*P*, calculated logarithm of the octanol-water partition coefficient; HBA, the number of hydrogen bond acceptor atoms; HBD, the number of hydrogen bond donor atoms; PSA, polar surface area; logBB = −0.0148 × PSA + 0.152 × *c*log*P* + 0.139 (logBB < −1.0, poorly distributed in the brain); $-\log P_e$ values, determined using the PAMPA-BBB assay, were calculated by PAMPA 9 explorer software v. 3.5. Compounds assigned to be CNS+ possess the ability to penetrate the BBB while those categorized as CNS− are expected to have poor BBB permeability.

Moreover, the toxicity of **bpy** derivatives was determined in human neuroblastoma SH-SY5Y (5Y) cells. Approximately 80% of cell survival was observed when 5Y cells were treated with the **bpy** derivatives (up to 50 μM) without metal ions for 24 h (Figure 2.10). In the presence of Zn(II) (5 or 10 μM), the **bpy** derivatives (up to 10 μM) exhibited *ca.* 85% of cell viability; however, upon incubation with Cu(II) (5 or 10 μM), they presented relatively moderate cytotoxicity (*ca.* 70% of cell survival; Figure 2.11). Note that due to compounds' toxicity with Cu(II), their ability to regulate toxicity triggered by metal–Aβ was not evaluated in living cells.

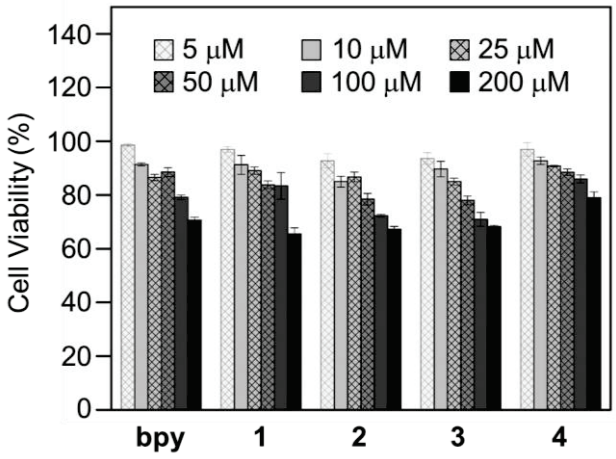

Figure 2.10. Toxicity of **bpy** and **1**–**4** in SH-SY5Y cells. Cells were treated with **bpy** or **1**–**4** for 24 h at 37 °C. Cell viability (%) was determined by the MTT assay. The viability values were calculated compared to those of cells added with DMSO only (1%, v/v). Error bars represent the standard error from three independent experiments ($P < 0.05$).

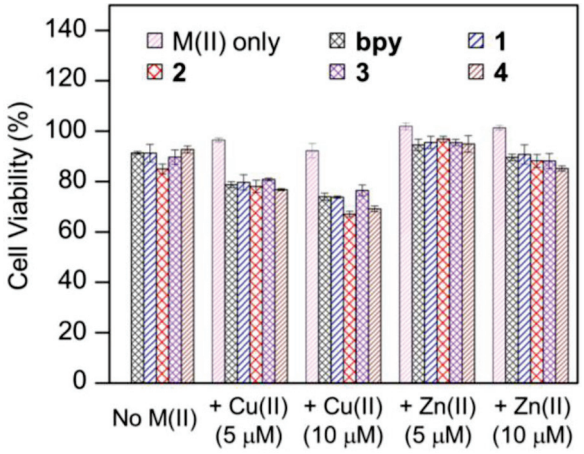

Figure 11. Toxicity of **bpy** and **1**–**4** in SH-SY5Y cells in the presence of metal ions. Cells were treated with **bpy** or **1**–**4** (10 μM) with metal ions (5 or 10 μM) for 24 h at 37 °C. Cell viability (%) was determined by the MTT assay. The viability values of cells were calculated compared to those of cells added with DMSO only (1%, v/v). Error bars represent the standard deviation from three independent experiments ($P < 0.05$).

2.3. Conclusions

Through a structure-based approach, new **bpy** derivatives (**1**–**4**) were rationally designed as chemical tools able to regulate metal–Aβ aggregation. The newly designed **bpy** derivatives were indicated to bind with Cu(II) and Zn(II) exhibiting different metal binding affinities, especially dependent on the location of the methyl substituent in the **bpy** framework. Moreover, our mass spectrometric studies presented the direct interactions, including the formation of a ternary Cu(II)–Aβ–**1** complex, of the **bpy** derivatives with Cu(II)–Aβ over metal-free Aβ. The structural modifications of **bpy** (*i.e.*, introduction of dimethylamino and methyl moieties) varied the characteristics of both metal binding and Aβ interaction, enabling the interaction between its derivatives and metal–Aβ, which in turn exhibited their noticeable reactivity towards control of metal–Aβ aggregation over metal-free Aβ analog. Alteration of metal-induced Aβ aggregation was also indicated by previously reported metal chelators, including 8-hydroxyquinoline (8-HQ) derivatives [*i.e.*, 8-HQ, clioquinol (CQ), PBT2].[7,18,48] Different from 8-HQ-based ligands shown to remove metal ions from metal–Aβ species, however, modulation of our **bpy** derivatives towards metal–Aβ aggregation is suggested to occur through chelating out metal ions from metal–Aβ species as well as forming a ternary complex with metal–Aβ. In order to fully elucidate how our **bpy** derivatives interact with Aβ and modulate Aβ aggregation, high-resolution structural studies with Aβ would be valuable to be pursued in the future. Our **bpy** derivatives were suggested to be BBB permeable but they displayed cytotoxicity at micromolar concentrations of Cu(II). Thus, further structural optimization of the derivatives is necessary for potential biological applications. Taken together, our studies demonstrate that chemical tools able to regulate metal–Aβ aggregation over metal-free Aβ analog can be developed *via* rational structure-

based design employing a backbone of a simple metal chelator. Our straightforward structural variations onto known metal chelating agents could be easily utilized to invent small molecules as chemical tools capable of interacting and reacting with metal-associated biological targets.

2.4. Experimental Section

2.4.1. Materials and Methods

All reagents were purchased from commercial suppliers and used as received unless otherwise noted. The ligand, **bpy**, was purchased from Sigma-Aldrich (St. Louis, MO, USA) and used without further purification. NMR and high-resolution mass spectrometric analyses of small molecules were conducted on an Agilent 400-MR DD2 NMR spectrometer (UNIST Central Research Facilities, Ulsan, Republic of Korea) and Q exactive plus orbitrap mass spectrometer (HRMS; Thermo Fisher Scientific, Waltham, MA, USA). Absorbance values for biological assays were measured on a Molecular Devices SpectraMax M5e microplate reader (Sunnyvale, CA, USA). Trace metal contamination was removed from buffers and solutions used for metal binding and Aβ experiments by treating with Chelex overnight (Sigma-Aldrich, St. Louis, MO, USA). Optical spectra were recorded on an Agilent 8453 UV−vis spectrophotometer. $A\beta_{40}$ and $A\beta_{42}$ were purchased from Anygen ($A\beta_{40}$ = DAEFRHDSGYEVHHQKLVFFAEDVGSNKGAIIGL-MVGGVV; Nam-myun, Jangseong-gun, Republic of Korea) and AnaSpec ($A\beta_{42}$ = DAEFRHDSGYEVH-HQKLVFFAEDVGSNKGAIIGLMVGGVVIA; Fremont, CA, USA), respectively. Double-distilled H_2O (ddH_2O) was obtained from a Milli-Q Direct 16 system (Merck KGaA, Darmstadt, Germany). ESI-MS and tandem MS analyses were performed using a Waters Synapt G2-Si quadrupole time-of-flight (Q-TOF) ion mobility mass spectrometer equipped with an ESI source (DGIST Center for Core Research Facilities, Daegu, Republic of Korea). TEM images were taken using a JEOL JEM-2100 transmission electron microscope (UNIST Central Research Facilities, Ulsan, Republic of Korea).

2.4.2. Synthesis Preparation

All reactions were carried out in flame or oven dried glassware under nitrogen atmosphere with freshly distilled dry solvents under anhydrous conditions unless otherwise indicated. Flash column chromatography was performed with silica gel 60 (230–400 mesh). Thin layer chromatography (TLC) plates were visualized by fluorescence quenching with UV light at 254 nm or by staining using base solution of potassium permanganate and molybdate. All reagents were obtained from commercial sources and were used without further purification.

2.4.3. *N,N*-Dimethyl-2-(tributylstannyl)pyridin-4-amine

To a solution of 2-dimethylamino-ethanol (146 mg, 1.64 mmol) in hexanes (4 mL) at –5 °C was added dropwise 2 M solution of *n*-BuLi (1.7 mL, 3.28 mmol) under nitrogen atmosphere and stirred at 0 °C

for 30 min. The solution was treated with 4-dimethylaminopyridine (100 mg, 0.8 mmol), stirred at 0 °C for 1 h, and cooled down to –78 °C. After addition of Bu_3SnCl (533 mg, 1.64 mmol), the reaction mixture was stirred at 0 °C for 1 h. The reaction mixture was quenched with water, and the aqueous phase was extracted with ether three times. The combined organic layers were dried over $MgSO_4$, filtered, and concentrated under reduced pressure. The crude product was purified by column chromatography using EtOAc as an eluent to give the stannylated product (78%) (EtOAc/NEt_3 = 99:1; R_f = 0.56). ^{1}H NMR (400 MHz, $CDCl_3$) / δ (ppm): 0.88 (9H, t, J = 7.3 Hz), 1.09 (6H, m), 1.33 (6H, dq, J = 14.5, 7.3 Hz), 1.57 (6H, dt, J = 15.8, 7.9 Hz), 2.97 (6H, s), 6.38 (1H, dd, J = 6.0, 2.9 Hz), 6.64 (1H, d, J = 2.9 Hz), 8.34 (1H, d, J = 6.0 Hz). ^{13}C NMR (100 MHz, $CDCl_3$) / δ (ppm): 9.7, 13.7, 27.4, 29.2, 38.9, 105.4, 115.5, 150.1, 152.1, 172.0. ESI-MS: Calcd for $C_{19}H_{36}N_2Sn$ $[M + H]^+$, 413.2; found 413.2.

2.4.4. General Procedure for 1–4

To a solution of *N,N*-dimethyl-2-(tributylstannyl)pyridin-4-amine (95 mg, 0.23 mmol) in toluene (2.5 mL) under nitrogen atmosphere was added $PdCl_2(PPh_3)_2$ (8 mg, 0.0115 mmol), LiCl (29 mg, 0.69 mmol), PPh_3 (6 mg, 0.023 mmol) and the appropriate bromide (2-bromopyridine, 2-bromo-*n*-methylpyridine, n = 4, 5, and 6; 1.2 mmol) and heated at 110 °C for 24 h. The reaction mixture was concentrated and purified by column chromatography.

2.4.5. *N,N*-Dimethylamino-(2,2'-bipyridin)-4-amine (1)

This compound was isolated by using column chromatography (EtOAc/NEt_3) as a white solid (50%). R_f (EtOAc/NEt_3 = 95:5) = 0.2. ^{1}H NMR (400 MHz, CD_2Cl_2) / δ (ppm): 3.09 (6H, s, *N-CH₃*), 6.56 (1H, dd, J = 5.9, 2.7 Hz, *H5*), 7.29 (1H, ddd, J = 7.5, 4.8, 1.2 Hz, *H5'*), 7.75 (1H, d, J = 2.7 Hz, *H3*), 7.80 (1H, td, J = 7.8, 1.8 Hz, *H4'*), 8.28 (1H, d, J = 5.9 Hz, *H6*), 8.40 (1H, dt, J = 8.0, 1.0 Hz, *H6'*), 8.63(1H, ddd, J = 4.8, 1.7, 0.9 Hz, *H3'*). ^{13}C NMR (100 MHz, $CDCl_3$) / δ (ppm): 39.1 (*N-CH₃*), 103.4 (*C5*), 106.6 (*C3*), 120.9 (*C3'*), 123.3 (*C5'*), 136.5 (*C6*), 148.7 (*C4'*), 149.2 (*C6'*), 155.2 (*C2'*), 155.9 (*C2*), 156.8 (*C4*). HRMS: Calcd for $C_{12}H_{14}N_3$ $[M + H]^+$, 200.1182; found 200.1180.

2.4.6. *N,N*,4'-Trimethyl-(2,2'-bipyridin)-4-amine (2)

This compound was obtained by using column chromatography (EtOAc/NEt_3) as a white solid (33%). R_f (EtOAc/NEt_3 = 99 :1) = 0.3. ^{1}H NMR (400 MHz, CD_2Cl_2) / δ (ppm): 2.43 (3H, s, *CH₃*), 3.09 (6H, s, *N-CH₃*), 6.55 (1H, dd, J = 5.8, 2.7 Hz, *H5*), 7.12 (1H, d, J = 4.4 Hz, *H5'*), 7.74 (1H, d, J = 2.7 Hz, *H3*), 8.27 (2H, d, J = 5.9 Hz, *H6* and *H6'*), 8.48 (1H, d, J = 4.9 Hz, *H3'*). ^{13}C NMR (100 MHz, CD_2Cl_2) / δ (ppm): 20.9 (*CH₃*), 39.1 (*N-CH₃*), 103.5 (*C5*), 106.5 (*C3*), 121.7 (*C5'*), 124.3(*C3'*), 147.8 (*C6*), 148.5 (*C4'*), 149.1 (*C6'*), 152.2 (*C2*), 156.0 (*C2'*), 156.6 (*C4*). HRMS: Calcd for $C_{13}H_{16}N_3$ $[M + H]^+$, 214.1339; found 214.1337.

2.4.7. *N*,*N*,5'-Trimethyl-(2,2'-bipyridin)-4-amine (3)

This compound was isolated by using column chromatography (EtOAc/NEt_3) as a white solid (42%). R_f (EtOAc/NEt_3 = 99 :1) = 0.2. ^{1}H NMR (400 MHz, CD_2Cl_2) / δ (ppm): 2.38 (3H, s, *CH*$_3$), 3.09 (6H, s, *N-CH*$_3$), 6.54 (1H, dd, *J* = 5.9, 2.7 Hz, *H5*), 7.61 (1H, ddd, *J* = 8.1, 2.2, 0.6 Hz, *H4'*), 7.71 (1H, d, *J* = 2.7 Hz, *H3*), 8.26 (1H, d, *J* = 5.9 Hz, *H6*), 8.29 (1H, d, *J* = 8.1 Hz, *H6'*), 8.46 (1H, m, *H3'*). ^{13}C NMR (100 MHz, CD_2Cl_2) / δ (ppm): 18.0 (*CH*$_3$), 39.1 (*N-CH*$_3$), 103.1 (*C5*), 106.4 (*C3*), 120.4 (*C3'*), 133.1 (*C5'*), 137.1 (*C6*), 148.9 (*C4'*), 149.2 (*C6'*), 154.1 (*C2'*), 155.2 (*C2*), 155.9 (*C4*). HRMS: Calcd for $C_{13}H_{16}N_3$ $[M + H]^+$, 214.1339; found 214.1337.

2.4.8. *N*,*N*,6'-Trimethyl-(2,2'-bipyridin)-4-amine (4)

This compound was isolated by using column chromatography (EtOAc/NEt_3) as a white solid (38%). R_f (EtOAc/NEt_3 = 99 :1) = 0.15. ^{1}H NMR (400 MHz, CD_2Cl_2) / δ (ppm): 2.61 (3H, s, *CH*$_3$), 3.09 (6H, s, *N-CH*$_3$), 6.55 (1H, dd, *J* = 5.9, 2.8 Hz, *H5*), 7.16 (1H, d, *J* = 7.6 Hz, *H5'*), 7.68 (1H, t, *J* = 7.7 Hz, *H4'*), 7.75 (1H, d, *J* = 2.7 Hz, *H3*), 8.17 (1H, d, *J* = 7.9 Hz, *H3'*), 8.27 (1H, d, *J* = 5.9 Hz, *H6*). ^{13}C NMR (100 MHz, CD_2Cl_2) / δ (ppm): 24.3 (*CH*$_3$), 39.4 (*N-CH*$_3$), 103.4 (*C5*), 106.5 (*C3*), 117.9 (*C5'*), 122.7 (*C3'*), 136.7 (*C6*), 149.1 (*C4'*), 155.2 (*C2*), 156.2 (*C4*), 157.5 (*C2'* and *C6'*). HRMS: Calcd for $C_{13}H_{16}N_3$ $[M + H]^+$, 214.1339; found 214.1336.

2.4.9. Parallel Artificial Membrane Permeability Adapted for the Blood–Brain Barrier (PAMPA-BBB) Assay

PAMPA-BBB experiments of compounds were conducted using the PAMPA Explorer kit (*p*ION, Inc. Billerica, MA, USA) with slight modifications of previously reported protocols.[21,25,28,45-47] Each compound stock solution was diluted with Prisma HT buffer (pH 7.4; *p*ION) to a final concentration of 25 μM [1% v/v dimethyl sulfoxide (DMSO)] and was added to the wells of the donor plate (200 μL, number of replicates = 12). BBB-1 lipid formulation (5 μL, *p*ION) was used to coat the polyvinylidene fluoride (PVDF, 0.45 μM) filter membrane on the acceptor plate. The acceptor plate was placed on top of the donor plate, forming a sandwich, and the brain sink buffer (BSB, 200 μL, *p*ION) was added to each well of the acceptor plate. The sandwich was incubated for 4 h at ambient temperature without stirring. UV−vis spectra of the solutions in the reference, acceptor, and donor plates were measured on a microplate reader. The PAMPA Explorer software, v. 3.5 (*p*ION), was used to calculate the value of $-\log P_e$ for each compound. CNS± designations were assigned by referring to compounds that were identified in previous reports.[45-47]

2.4.10. Metal Binding Experiments

Metal binding of **bpy** and **1**–**4** was investigated by UV−vis. UV−vis experiments were carried out in the Chelex-treated buffered solution (20 μM HEPES, pH 7.4, 150 μM NaCl). To a solution of a ligand, $CuCl_2$ or $ZnCl_2$ was titrated up to 5 equiv at room temperature. The solution was stabilized to equilibrate for 5 min after addition of compounds. The spectra were recorded after 5 min incubation at room temperature.

2.4.11. Solution Speciation Studies

The pK_a values for **bpy** and **1**–**4** were determined through UV−vis variable-pH titrations based on previously reported procedures.[21,27,28] To obtain pK_a values for compounds, the solution of compound (25 μM; 10 mM NaOH, pH 12, 100 mM NaCl) was titrated with in small aliquots of HCl to obtain at least 30 spectra in a range of pH 3.5 to 10. In addition, to determine the binding affinities of compounds to Cu(II) or Zn(II), small aliquots of HCl were titrated into their solution containing ligand and a metal chloride salt [[M(II)]:[L] = 1:2; [Cu(II)] = 12.5 μM, [Zn(II)] = 12.5 (for **bpy** and **1**–**3**) or 50 μM (for **4**)]. At least 30 spectra were acquired over the pH range (3.5−8). The acidity and stability constants were calculated by the HypSpec program (Protonic Software, Leeds, UK).[49,50]

2.4.12. Electrospray Ionization Mass Spectrometry (ESI-MS)

$A\beta_{40}$ (100 μM) was incubated with compounds (**bpy** and **1**–**4**, 500 μM) for 1 h at 37 °C without agitation [20 mM ammonium acetate, pH 7.2 (with 1% v/v DMSO)] in the absence and presence of $CuCl_2$ (100 μM). Before the injection of samples into the mass spectrometer, the incubated samples were diluted by 10 fold. ESI-MS analysis was performed using the Synapt G2-Si Q-TOF mass spectrometer (Waters, Manchester, UK) equipped with ESI source. The capillary voltage, sampling cone voltage, and source temperature were set to 2.8 kV, 40 V, and 40 °C, respectively. Tandem MS analysis was also performed based on the same instrumental conditions. The isolation width was set as approximately 5 by adjusting low mass resolution to 4.7, and 15 eV collision energy was applied to the trap cell to dissociate the precursor ion.

2.4.13. Aβ Aggregation Experiments

All experiments were performed according to previously published methods.[21,27,28,34] Prior to experiments, $A\beta_{40}$ or $A\beta_{42}$ was dissolved in ammonium hydroxide (NH_4OH, 1% v/v, aq), aliquoted, lyophilized overnight, and stored at −80 °C. For experiments described herein, a stock solution of Aβ was prepared by dissolving the lyophilized peptide in 1% NH_4OH (10 μL) and diluting with ddH_2O. The concentration of Aβ was determined by measuring the absorbance of the solution at 280 nm (ε = 1450 M^{-1} cm^{-1} for $A\beta_{40}$; ε = 1490 M^{-1} cm^{-1} for $A\beta_{42}$). The peptide stock solution was diluted to a

final concentration of 25 μM in the Chelex-treated buffered solution containing HEPES [20 μM; pH 7.4 (for metal-free and Zn(II) samples) or pH 6.6 (for Cu(II) samples)] and NaCl (150 μM). For the studies, a compound (final concentration, 50 μM; 1% v/v DMSO) was added to the sample of Aβ (25 μM) in the absence and presence of a metal chloride salt ($CuCl_2$ or $ZnCl_2$; 25 μM) followed by incubation for 24 h at 37 °C with constant agitation.

2.4.14. Gel Electrophoresis with Western Blot

The samples from Aβ experiments were analyzed by gel electrophoresis with Western blotting using an anti-Aβ antibody (6E10).[21,27,28,34] Each sample (10 μL) was separated on a 10−20% Tris-tricine gel (Thermo Fisher Scientific, Carlsbad, CA, USA). Following separation, the proteins were transferred onto nitrocellulose membrane, which was blocked with bovine serum albumin (BSA, 3% w/v, RMBIO, Missoula, MT, USA) in Tris-buffered saline (TBS) containing 0.1% Tween-20 (TBS-T) for 2 h at room temperature. The membranes were incubated with the antibody (6E10), (1:2,000; Covance, Princeton, NJ, USA) in a solution of 2% BSA (w/v in TBS-T) overnight at 4 °C. After washing, the horseradish peroxidase-conjugated goat antimouse secondary antibody (1:5,000) in 2% BSA was added for 1 h at room temperature. A homemade ECL kit[51] was used to visualize the results on a ChemiDoc MP Imaging System (Bio- Rad, Hercules, CA, USA).

2.4.15. Transmission Electron Microscopy (TEM)

Samples for TEM were prepared according to previously reported methods.[21,27,28,34,35] Glow-discharged grids (Formvar/Carbon 300-mesh, Electron Microscopy Sciences, Hatfield, PA, USA) were treated with Aβ samples from the experiments (5 μL) for 2 min at room temperature. Excess sample was removed using filter paper followed by washing three times with ddH_2O. Each grid was incubated with uranyl acetate (1% w/v ddH_2O, 5 μL) for 1 min. Upon removal of excess uranyl acetate with filter paper, the grids were dried for at least 20 min at room temperature before measurement. Images from each sample were taken on a JEOL JEM-2100 transmission electron microscope (200 kV; 25,000x magnification).

2.4.16. Cell Viability Measurements

The human neuroblastoma SH-SY5Y cell line was purchased from the American Type Cell Collection (ATCC, Manassas, VA, USA). Cells were maintained in media containing 1:1 Minimum Essential Media (MEM; GIBCO, Grand Island, NY, USA) and Ham's F12K Kaighn's Modification Media (F12 K; GIBCO), 10% (v/v) fetal bovine serum (FBS; GIBCO), and 1 U/mL penicillin (GIBCO). The cells were grown and maintained at 37 °C in a humidified atmosphere with 5% CO_2. Cell viability upon treatment with compounds was determined by the MTT assay [MTT = 3-(4,5-

dimethyl-2-thiazolyl)-2,5-diphenyl-2*H*-tetrazolium bromide, Sigma-Aldrich]. SH-SY5Y cells were seeded in a 96 well plate (15,000 cells in 100 μL per well). The cells were treated with compounds (5 or 10 μM, 1% v/v final DMSO concentration) with or without $CuCl_2$ or $ZnCl_2$ (5 or 10 μM), and incubated for 24 h. After incubation, MTT [25 μL; 5 mg/mL in phosphate buffered saline (PBS, pH 7.4, GIBCO)] was added to each well, and the plate was incubated for 4 h at 37 °C. Formazan produced by the cells was solubilized using an acidic solution of *N*,*N*-dimethylformamide (DMF, 50% v/v aq) and sodium dodecyl sulfate (SDS, 20% w/v) overnight at room temperature in the dark. The absorbance was measured at 600 nm using a microplate reader. Cell viability was calculated relative to cells treated with an equivalent amount of DMSO. All experiments were carried out in triplicate.

2.5. Acknowledgments

This work was supported by the 2017 Research Fund (Project Number 1.170014.01) of Ulsan National Institute of Science and Technology (UNIST) (to C.-M.P. and M.H.L.); the Nine Bridges Program Research Fund (Project Number 1.170051.01) of UNIST (to M.H.L.); the National Research Foundation of Korea (NRF) grant funded by the Korean government (NRF-2017R1A2B3002585) (to M.H.L.); the DGIST R&D Program (17-BD-0403) (to J.C.).

2.6. References

(1) Prince, M.; Comas-Herrera, A.; Knapp, M.; Guerchet, M.; Karagiannidou, M. *World Alz heimer Report 2016*; Alzheimer's Disease International: London, U.K., **2016**

(2) Jakob-Roetne, R.; Jacobsen, H. *Angew. Chem. Int. Ed.* **2009**, *48*, 3030–3059.

(3) Hamley, I. W. *Chem. Rev.* **2012**, *112*, 5147–5192.

(4) Kepp, K. P. *Chem. Rev.* **2012**, *112*, 5193–5239.

(5) Lee, S. J. C.; Nam, E.; Lee, H. J.; Savelieff, M. G.; Lim, M. H. *Chem. Soc. Rev.* **2017**, *46*, 310–323.

(6) Savelieff, M. G.; Lee, S.; Liu, Y.; Lim, M. H. *ACS Chem. Biol.* **2013**, *8*, 856–865.

(7) Beck, M. W.; Pithadia, A. S.; DeToma, A. S.; Korshavn, K. J.; Lim, M. H. *Ligand Design in Medicinal Inorganic Chemistry*; Storr, T., Eds.; Wiley: Chichester, U.K., 2014; Chapter 10, pp 257-286.

(8) Derrick, J. S.; Lim, M. H. *ChemBioChem* **2015**, *16*, 887–898.

(9) Kotler, S. A.; Walsh, P.; Brender, J. R.; Ramamoorthy, A. *Chem. Soc. Rev.* **2014**, *43*, 6692–6700.

(10) Faller, P. *ChemBioChem* **2009**, *10*, 2837–2845.

(11) Faller, P.; Hureau, C. *Dalton Trans.* **2009**, 1080–1094.

(12) Telpoukhovskaia, M. A.; Orvig, C. *Chem. Soc. Rev.* **2013**, *42*, 1836–1846.

(13) Zatta, P.; Drago, D.; Bolognin, S.; Sensi, S. L. *Trends Pharmcol. Sci.* **2009**, *30*, 346–355.

(14) Barnham, K. J.; Bush, A. I. *Chem. Soc. Rev.* **2014**, *43*, 6727–6749.

(15) Ayton, S.; Lei, P.; Bush, A. I. *Neurotherapeutics* **2015**, *12*, 109–120.

(16) Tõugu, V.; Tiiman, A.; Palumaa, P. *Metallomics* **2011**, *3*, 250–261.

(17) Savelieff, M. G.; DeToma, A. S.; Derrick, J. S.; Lim, M. H. *Acc. Chem. Res.* **2014**, *47*, 2475–2482.

(18) Adlard, P. A.; Cherny, R. A.; Finkelstein, D. I.; Gautier, E.; Robb, E.; Cortes, M.; Volitakis, I.; Liu, X.; Smith, J. P.; Perez, K.; Laughton, K.; Li, Q.-X.; Charman, S. A.; Nicolazzo, J. A.; Wilkins, S.; Deleva, K.; Lynch, T.; Kok, G.; Ritchie, C. W.; Tanzi, R. E.; Cappai, R.; Masters, C. L.; Barnham, K. J.; Bush, A. I. *Neuron* **2008**, *59*, 43–55.

(19) Choi, J.-S.; Braymer, J. J.; Nanga, R. P. R.; Ramamoorthy, A.; Lim, M. H. *Proc. Natl. Acad. Sci. U. S. A.* **2010**, *107*, 21990–21995.

(20) Sharma, A. K.; Pavlova, S. T.; Kim, J.; Finkelstein, D.; Hawco, N. J.; Rath, N. P.; Kim, J.; Mirica, L. M. *J. Am. Chem. Soc.* **2012**, *134*, 6625–6636.

(21) Lee, S.; Zheng, X.; Krishnamoorthy, J.; Savelieff, M. G.; Park, H. M.; Brender, J. R.; Kim, J. H.; Derrick, J. S.; Kochi, A.; Lee, H. J.; Kim, C.; Ramamoorthy, A.; Bowers, M. T.; Lim, M. H. *J. Am. Chem. Soc.* **2014**, *136*, 299–310.

(22) Gonzalez, P.; da Costa, V. C. P.; Hyde, K.; Wu, Q.; Annunziata, O.; Rizo, J.; Akkaraju, G.; Green, K. N. *Metallomics* **2014**, *6*, 2072–2082.

(23) Lincoln, K. M.; Richardson, T. E.; Rutter, L.; Gonzalez, P.; Simpkins, J. W.; Green, K. N. *ACS Chem. Neurosci.* **2012**, *3*, 919–927.

(24) Beck, M. W.; Oh, S. B.; Kerr, R. A.; Lee, H. J.; Kim, S. H.; Kim, S.; Jang, M.; Ruotolo, B. T.; Lee, J.-Y.; Lim, M. H. *Chem. Sci.* **2015**, *6*, 1879–1886.

(25) Derrick, J. S.; Kerr, R. A.; Nam, Y.; Oh, S. B.; Lee, H. J.; Earnest, K. G.; Suh, N.; Peck, K. L.; Ozbil, M.; Korshavn, K. J.; Ramamoorthy, A.; Prabhakar, R.; Merino, E. J.; Shearer, J.; Lee, J.-Y.; Ruotolo, B. T.; Lim, M. H. *J. Am. Chem. Soc.* **2015**, *137*, 14785–14797.

(26) Hevroni, B. L.; Major, D. T.; Dixit, M.; Mhashal, A. R.; Das, S.; Fischer, B. *Org. Biomol. Chem.* **2016**, *14*, 4640–4653.

(27) Derrick, J. S.; Kerr, R. A.; Korshavn, K. J.; McLane, M. J.; Kang, J.; Nam, E.; Ramamoorthy, A.; Ruotolo, B. T.; Lim, M. H. *Inorg. Chem.* **2016**, *55*, 5000–5013.

(28) Beck, M. W.; Derrick, J. S.; Kerr, R. A.; Oh, S. B.; Cho, W. J.; Lee, S. J. C.; Ji, Y.; Han, J.; Tehrani, Z. A.; Suh, N.; Kim, S.; Larsen, S. D.; Kim, K. S.; Lee, J.-Y.; Ruotolo, B. T.; Lim, M. H. *Nat. Commun.* **2016**, *7*, 13115.

(29) Maqsood, S. R.; Islam, N.; Bashir, S.; Khan, B.; Pandith, A. H. *J. Coord. Chem.* **2013**, *66*, 2308–2315.

(30) Irving, H. M.; Williams, R. J. P. *Analyst* **1952**, *77*, 813–829.

(31) Holyer, R. H.; Hubbard, C. D.; Kettle, S. F. A.; Wilkins, R. G. *Inorg. Chem.* **1965**, *4*, 929–935.

(32) Sone, K.; Krumholz, P.; Stammreich, H. *J. Am. Chem. Soc.* **1955**, *77*, 777–780.

(33) Kung, H. F.; Lee, C.-W.; Zhuang, Z.-P.; Kung, M.-P.; Hou, C.; Plössl, K. *J. Am. Chem. Soc.* **2001**, *123*, 12740–12741.

(34) Lee, H. J.; Korshavn, K. J.; Nam, Y.; Kang, J.; Paul, T. J.; Kerr, R. A.; Youn, I. S.; Ozbil, M.; Kim, K. S.; Ruotolo, B. T.; Prabhakar, R.; Ramamoorthy, A.; Lim, M. H. *Chem. Eur. J.* **2017**, *23*, 2706–2715.

(35) Kang, J.; Lee, S. J. C.; Nam, J. S.; Lee, H. J.; Kang, M.-G.; Korshavn, K. J.; Kim, H.-T.; Cho, J.; Ramamoorthy, A.; Rhee, H.-W.; Kwon, T.-H.; Lim, M. H. *Chem. Eur. J.* **2017**, *23*, 1645–1653.

(36) Dewick, P. M. *Essentials of organic chemistry: for students of pharmacy, medicinal chemistry and biological chemistry*: Wiley: Hoboken, NJ, 2006; Chapter 4.

(37) Hoste, J. *Anal. Chim. Acta* **1950**, *4*, 23–37.

(38) Yalkowsky, S. H.; Dannenfelser, R. M. *The aquasol database of aqueous solubility*; College of Pharmacy, University of Arizona, Tucson, AZ, **1992**.

(39) Wu, H.; Wu, T.; Li, M.; Wang, J. *Neurobiol. Dis.* **2012**, *45*, 388–394.

(40) Hommes, P.; Reissig, H.-U. *Beilstein J. Org. Chem.* **2016**, *12*, 1170–1177.

(41) Imamura, T.; Hirayama, T.; Tsuruma, K.; Shimazawa, M.; Nagasawa, H.; Hara, H. *Exp. Eye Res.* **2014**, *129*, 24–30.

(42) Jin, A.; Lee, J. N.; Kim, M. S.; Kwak, S.; Kim, S.-J.; Song, K.; Choe, S.-K.; Park, R. *Biochem. Biophys. Res. Commun.* **2016**, *469*, 941–947.

(43) Stille, J. K. *Angew. Chem. Int. Ed.* **1986**, *25*, 508–524.

(44) Fujita, M.; Oka, H.; Ogura, K. *Tetrahedron Lett.* **1995**, *36*, 5247–5250.

(45) Di, L.; Kerns, E. H.; Fan, K.; McConnell, O. J.; Carter, G. T. *Eur. J. Med. Chem.* **2003**, *38*, 223–232.

(46) Avdeef, A.; Bendels, S.; Di, L.; Faller, B.; Kansy, M.; Sugano, K.; Yamauchi, Y. *J. Pharm. Sci.* **2007**, *96*, 2893–2909.

(47) *BBB Protocol and Test Compounds*; *p*ION Inc.: Woburn, MA, **2009**.

(48) Dickens, M. G.; Franz, K. J. *ChemBioChem* **2010**, *11*, 59–62.

(49) Gans, P.; Sabatini, A.; Vacca, A. *Ann. Chim.* **1999**, *89*, 45–49.

(50) Alderighi, L.; Gans, P.; Ienco, A.; Peters, D.; Sabatini, A.; Vacca, A. *Coord. Chem. Rev.* **1999**, *184*, 311–318.

(51) Mruk, D. D.; Cheng, C. Y. *Spermatogenesis* **2011**, *1*, 121–122.

Appendix A.

Synthesis of ΔFosB Inhibitor

A.1. introduction

The ΔFosB is a transcription factor, kind of leucine zipper working dimeric form.[1] It is accumulated in striatum of the brain, and related in gene expression and accumulates in human body.[1,2] The elevated levels of ΔFosB are thought to mediate long-lasting neural and behavioral changes in response to drug addiction and dyskinesia.[3-5] The ΔFosB also mediates endogenous resilience or handling mechanisms of stress.[6] To inhibit the elevated level of ΔFosB, large number of small molecules were screened.[7]

Two active analogues were identified to inhibit ΔFosB with micromolar concentration of IC_{50} value.[7] The IC_{50} values of them were too high to apply in the human body.[7] For increasing their reactivity, structures of small molecules were modified.[7] To enhance the reactivity of ΔFosB inhibitor, structure variations were applied to ΔFosB inhibitors.[7] The newly prepared molecules, however, were shown slightly better IC_{50} value with before or poorer.[7] Herein, the design and synthesis of ΔFosB inhibitor which two reactive moiety connected by linker will be described.

A.2. Result and Discussion

To enhance the IC_{50} value, structure modified molecules were prepared and tested, however, the IC_{50} values of them are still shown micromolar range.[7] For better reactivity, two individual ΔFosB inhibitor (**C6**) are connected by linker. The **C6** are connected by linker (*e.g.*, different length of alkyl chain). First, (Z)-5-(5-hydroxy-2-nitrobenzylidene)-2-thioxo-thiazolidin-4-one (**C6-OH**) were prepared by Knoevenagel condensation reaction with the 5-hydroxy-2-nitrobenzaldehyde and 2-thioxothiazolidin-4-one.[8,9] **C6-OH** was then deprotonated in the KOH solution to produce the potassium (Z)-4-nitro-3-((4-oxo-2-thioxothiazolidin-5-ylidene)methyl)phenolate (**C6-OK**). The (5Z,5'Z)-5,5'-(((butane-1,4-diylbis(oxy))bis(6-nitro-3,1-phenylene))bis(methanylylidene))bis(2-thioxothiazolidin-4-one) (**C6-n2m**) and 5-((Z)-5-hydroxy-2-nitrobenzylidene)-3-(10-(4-nitro-3-((Z)-(4-oxo-2-thioxothiazolidin-5-ylidene)methyl)phenoxy)decyl)-2-thioxothiazolidin-4-one (**C6-n4m**) was constructed by Williamson ether synthesis **C6-OK** with either 1,4-dibromobutane or 1,10-dibromodecane respectively as shown in scheme A.1.[10]

Shceme A.1. Synthetic routes to **C6-n2m** and **C6-n4m**.

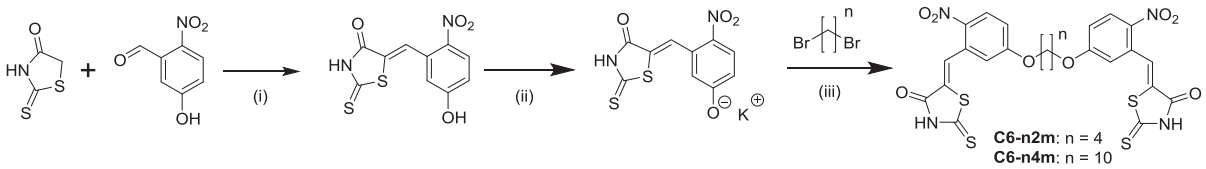

Ragents and conditions: (i) β-alanine, acetic acid, 100 °C, yield: 72%; (ii) KOH, EtOH, rt, yield: 37%; (iii) DMF, 80 °C, yield: 27%.

A.3. Experimental Section

A.3.1. Syntheses

The compounds, 5-hydroxy-2-nitrobenzaldehyde and 2-thioxothiazolidin-4-one were purchased from alfa aesar, 1,4-dibromobutane and 1,10-dibromodecane were purchased from TCI chemicals.

A.3.2. (Z)-5-(5-hydroxy-2-nitrobenzylidene)-2-thioxothiazolidin-4-one (C6-OH)

A solution of acetic acid (15 mL) was added 5-hydroxy-2-nitrobenzaldehyde (517 mg, 3 mmol), 2-thioxothiazolidin-4-one (815 mg, 6 mmol), and β-alanine (847 mg, 6 mmol). The reaction mixture was heating to 100 °C with stirring for 3 h. After 3 h, the reaction mixture was cooling down in the ice bath. Generated powder was filtered and washing with water. The powder was recrystallized in acetone/H_2O to afford the product (yellow powder, 610 mg, 2.16 mmol, 72% yield). ^{1}H NMR (400 MHz, $(CD_3)_2SO$ / δ (ppm): 13.89 (1H, s), 11.31 (1H, s), 8.14 (1H, d, J = 8.83 Hz), 7.88 (1H, s), 6.98 (2H, m).

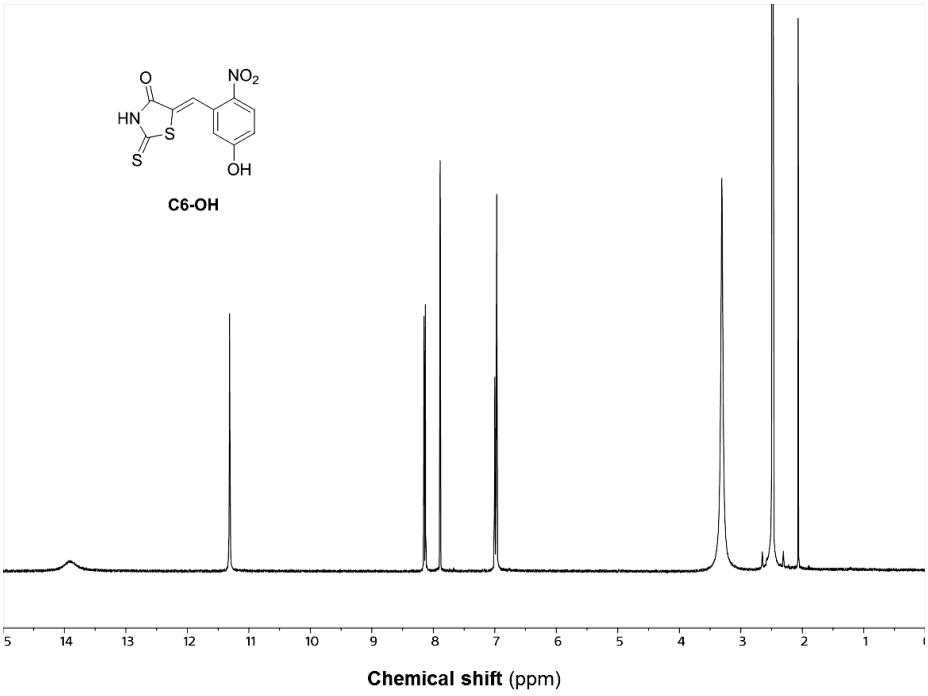

Figure A.1. ^{1}H NMR spectrum of **C6-OH** [400 MHz, $(CD_3)_2SO$]

A.3.3. Potassium (Z)-4-nitro-3-((4-oxo-2-thioxothiazolidin-5-ylidene)methyl)phenolate (C6-OK)

A solution of EtOH (15 mL) was added KOH (140 mg, 2.48 mmol) and (Z)-5-(5-hydroxy-2-nitrobenzylidene)-2-thioxothiazolidin-4-one (**C6-OH**) (642 mg, 2.27 mmol). The reaction mixture was allowed to stir for 3 h. The product was filtered and washed with EtOH (orange powder, 268 mg, 0.84 mmol, 37% yield). ^{1}H NMR (400 MHz, $(CD_3)_2SO$ / δ (ppm): 7.91 (1H, d, J = 9.29 Hz), 7.50 (1H, s), 6.53 (1H, s), 6.41 (1H, d, J = 9.23 Hz).

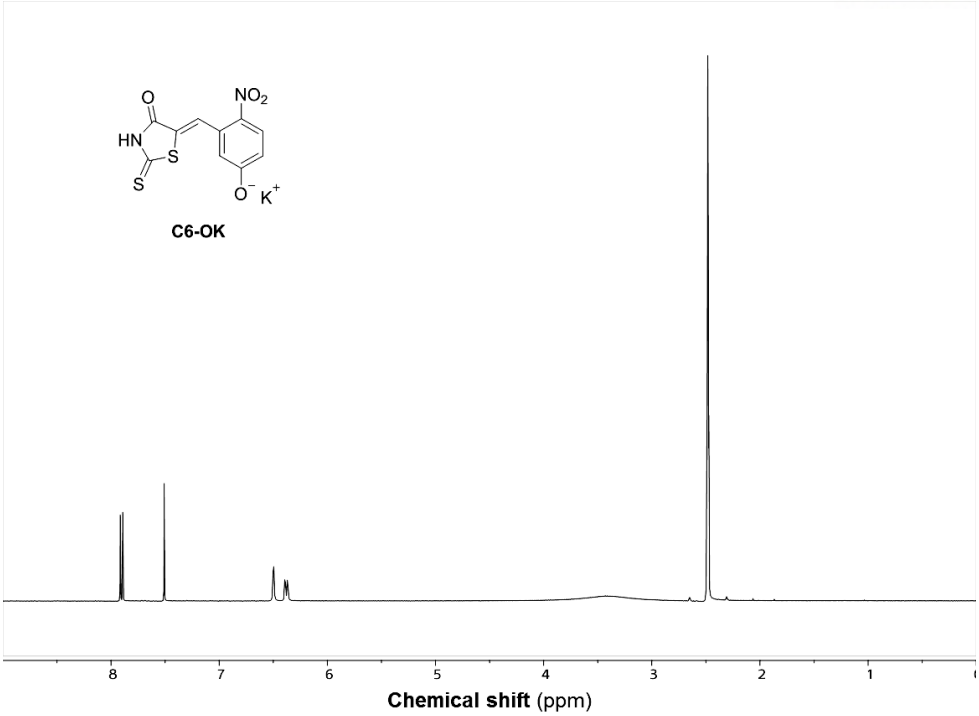

Figure A.2. ^{1}H NMR spectrum of **C6-OK** [400 MHz, $(CD_3)_2SO$]

A.3.4.The (5Z,5'Z)-5,5'-(((butane-1,4-diylbis(oxy))bis(6-nitro-3,1-phenylene))bis(methanylylidene))bis(2-thioxothiazolidin-4-one) (C6-n2m)

The **C6-OK** (471 mg, 1.47 mmol) was dissolved in dried DMF (5 mL) and stirred in the flask. Then 1,4-dibromobutane (58.5 μL, 0.49 mmol) was added drop-wise. The reaction mixture was refluxed at 80 °C under the N_2 condition for 6 h. After the reaction, the mixture was extracted EtOAc/water. The organic layer was collected, washed with brine, dried with $MgSO_4$, filtered and concentrated. The crude was purified by column chromatography (SiO_2, 1:1 hexanes/EtOAc, R_f = 0.4). The final product (pale yellow powder) was obtained. (80 mg, 1.5 mmol, 27% yield). ^{1}H NMR (400 MHz, $(CD_3)_2SO$ / δ (ppm): 11.34 (2H, s), 8.14 (2H, d, J = 9.26 Hz), 8.05, (2H, s), 7.00 (4H, m), 4.04 (4 H, s), 1.72 (4H, s). ^{13}C NMR (100 MHz, $(CD_3)_2SO$ / δ (ppm): 194.3, 166.7, 163.3, 139.8, 132.3, 130.7, 129.2, 127.2, 1177, 115.7, 44.4, 24.2. ESI-MS Calcd for $C_{24}H_{17}N_4O_8S_4$ $[M-H]^-$, 617.994; found 617.161.

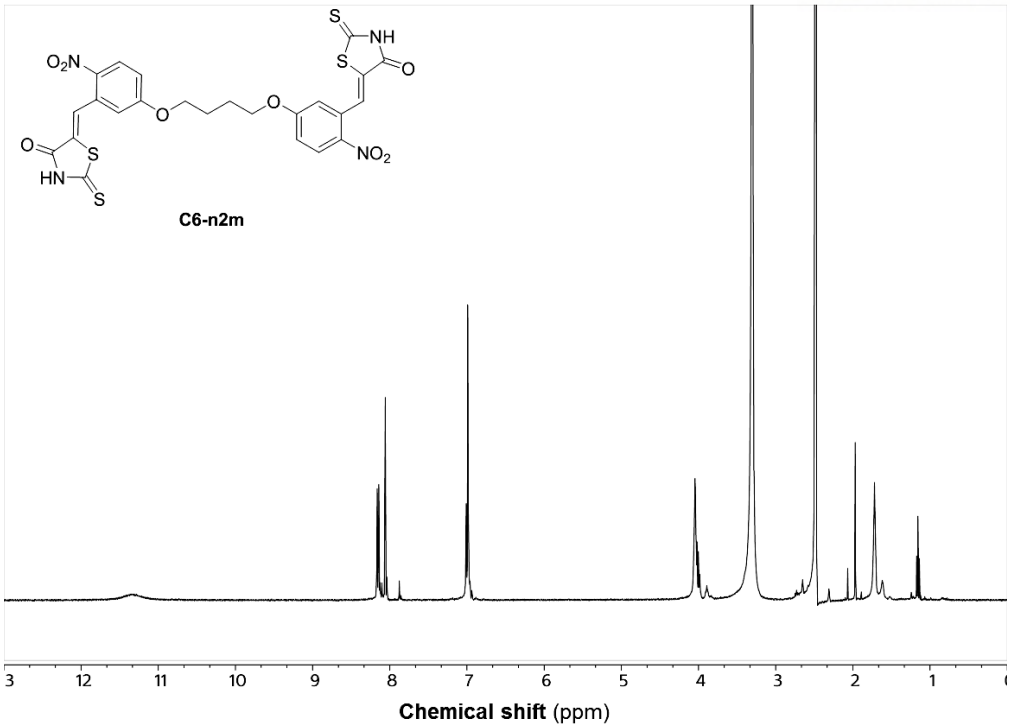

Figure A.3. ^{1}H NMR spectrum of **C6-n2m** [400 MHz, $(CD_3)_2SO$]

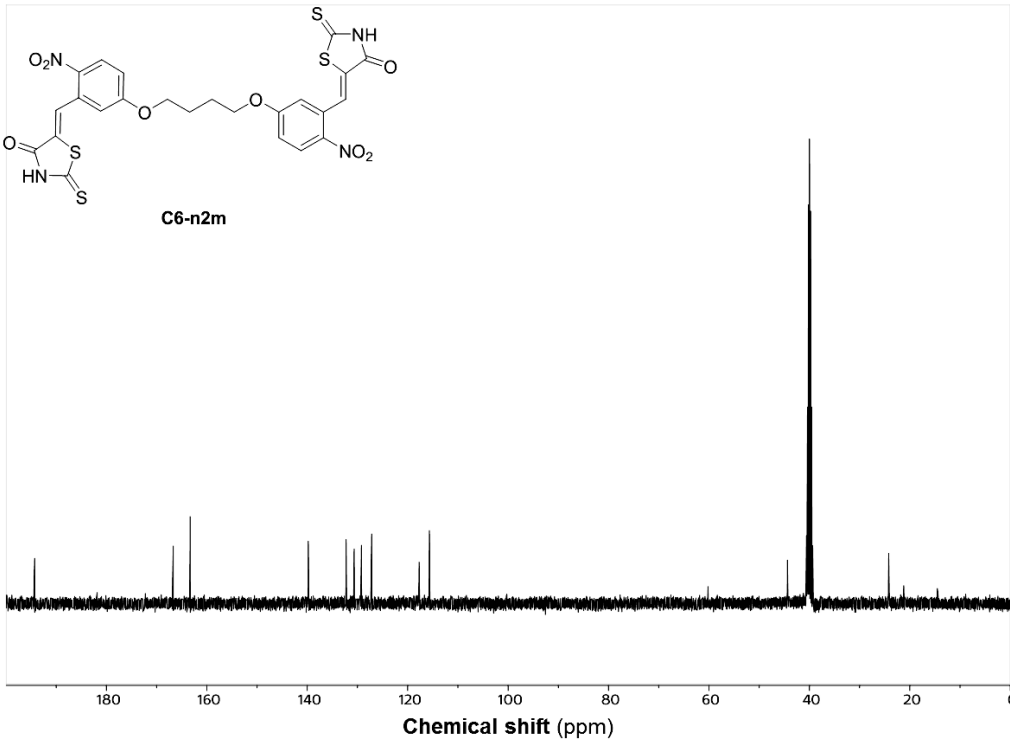

Figure A.4. ^{13}C NMR spectrum of **C6-OK** [100 MHz, $(CD_3)_2SO$]

A.3.5. 5-((Z)-5-hydroxy-2-nitrobenzylidene)-3-(10-(4-nitro-3-((Z)-(4-oxo-2-thioxothiazolidin-5-ylidene)methyl)phenoxy)decyl)-2-thioxothiazolidin-4-one (C6-n4m')

The **C6-OK** (320 mg, 1.07 mmol) was dissolved in dried DMF (5 mL) and stirred in the flask. Then 1,10-dibromodecane (89.1 μL, 0.43 mmol) was added drop-wise. The reaction mixture was refluxed at 80 °C under the N_2 condition for 3 h. After the reaction, the mixture was extracted EtOAc/water. The organic layer was collected, washed with brine, dried with $MgSO_4$, filtered and concentrated. The crude was purified by column chromatography (SiO_2, 1:1 hexanes/EtOAc, R_f = 0.24). The final product (yellow powder) was obtained. (80 mg, 1.5 mmol, 27% yield). ^{1}H NMR (400 MHz, $(CD_3)_2SO$ / δ(ppm): 11.34 (2H, s), 8.14 (4H, m), 8.07 (1H, s), 8.05 (1H, s), 6.99 (4H, m), 3.99 (4H, s), 1.62 (4H, s), 1.27 (12H, m). ^{13}C NMR (100 MHz, $(CD_3)_2SO$ / δ(ppm): 194.2, 193.8, 178.2, 166.6, 163.7, 139.6, 133.6, 133.2, 132.3, 131.1, 130.8, 129.2, 129.0, 117.8, 117.6, 116.0, 115.8, 44.8, 33.6, 29.1, 28.9, 28.8, 28.3, 26.6, 26.5. ESI-MS Calcd for $C_{30}H_{29}N_4O_8S_4$ $[M-H]^-$, 701.087; found 701.359.

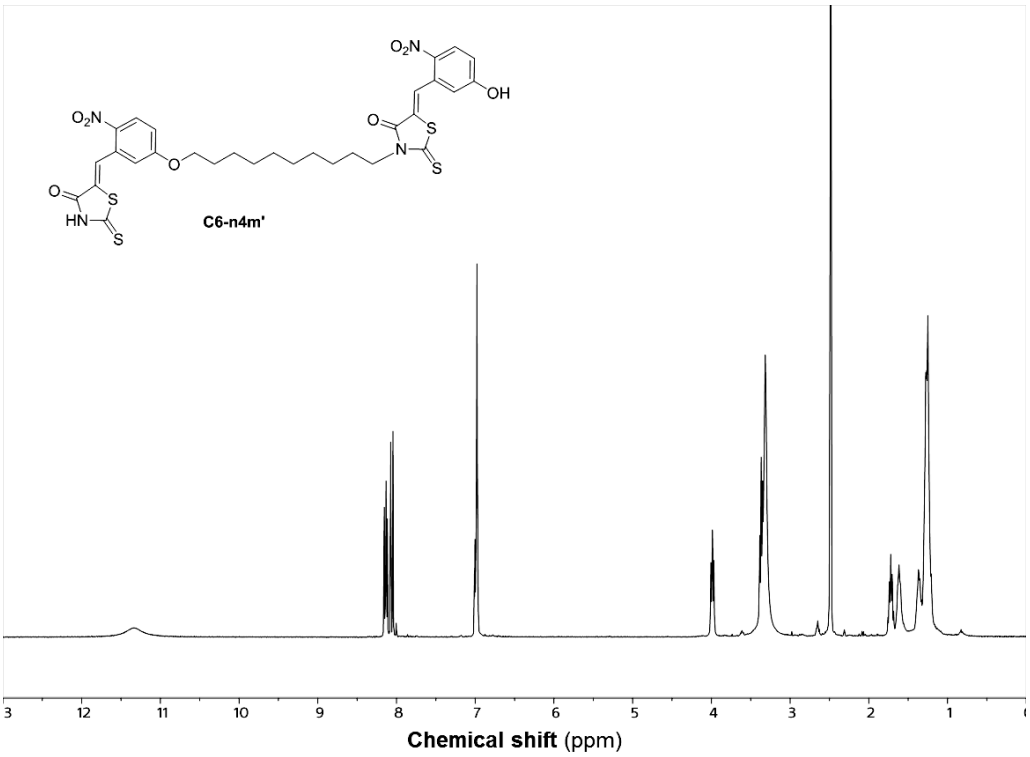

Figure A.5. ^{1}H NMR spectrum of **C6-n4m'** [400 MHz, $(CD_3)_2SO$]

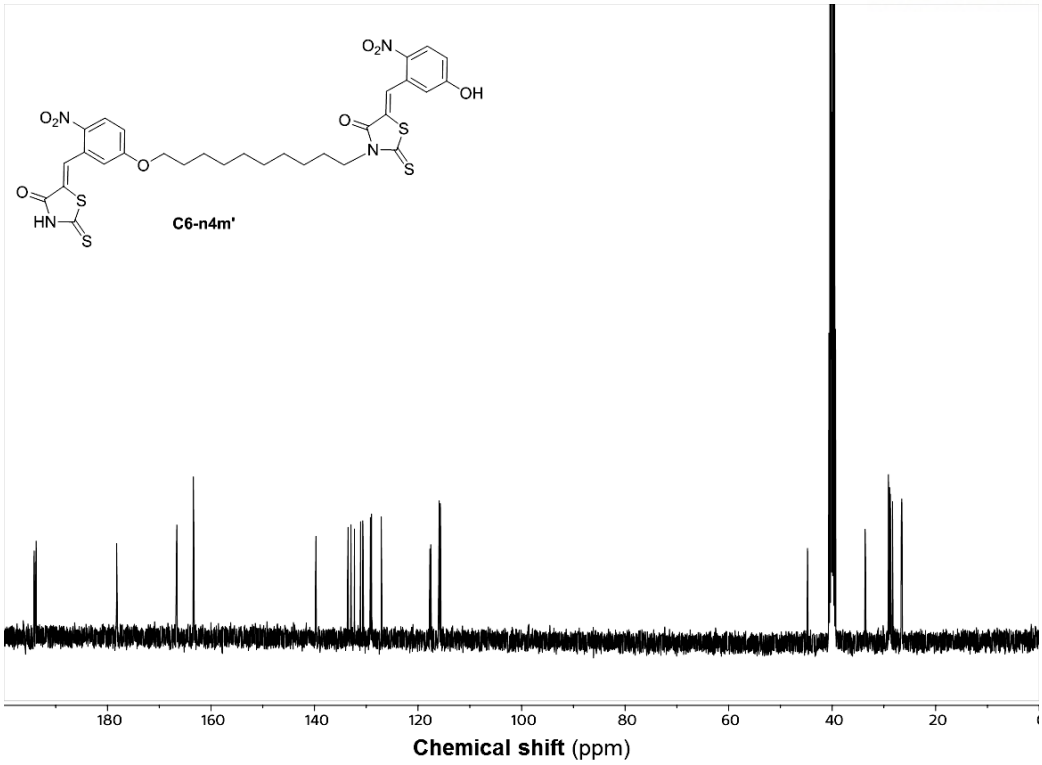

Figure A.6. ^{13}C NMR spectrum of **C6-n4m'** [100 MHz, $(CD_3)_2SO$]

A.4. Conclusion

The ΔFosB, one of transcription factor, mediates endogenous resilience or handling mechanisms of stress. Overproduced ΔFosB, however, is involved in drug addiction and diyskinesia. To inhibit the elevated level of ΔFosB, designed inhibitor (**C6**) was developed by connection with linker. Newly synthesized compounds (**C6-n2m** and **C6-n4m**) are expected to show the lower IC_{50} value than **C6** analogue. The binding position of ΔFosB with protein also could be predicted by length of linker. This work might be helpful for future work to develop the ΔFosB inhibitor.

A.5. Acknowledgments

This work was supported by the 2017 Research Fund (Project Number 1.170014.01) of Ulsan National Institute of Science and Technology (UNIST) (to M.H.L.); the Nine Bridges Program Research Fund (Project Number 1.170051.01) of UNIST (to M.H.L.); the National Research Foundation of Korea (NRF) grant funded by the Korean government (NRF-2017R1A2B3002585) (to M.H.L).

A.5. References

Acknowledgement

Completion of this thesis was impossible without the assistance, support, guidance and encouragements of many people. I would love to express my sincere gratitude to them.

Foremost, I would thank for my advisor, Professor Mi Hee Lim for her guidance and supporting during my M.S. course. Without her advisements and assistance, I never finish it. Furthermore, published the paper or finish the projects was possible with her guidance, advisement, and scientific discussion. She was always allowed to use her valuable time for our lab and members. Without her hardworking and sacrificing, Our lab will not work well. During M.S. course, I learned a lot of things from her, that not only several experiments, scientific writing and thinking, but also leadership, common sense. She is the person who most affect my life. My value of my life was changed during my M.S. course with my characters. It was lucky to join the Lim lab and meet the great advisor. I really appreciate to her.

I also want to thank all of my Lim Lab group members, including past members, for their assistance, friendship, encouragement and scientific discussion. In particular, thank for Dr. Akkiko Kochi, Dr. Michael Beck, Dr. Shin Jung Lee, Dr. Hyuck Jin Lee, Juhye Kang, Geewoo Nam, Jeffrey S. Derrick, Eunju Nam, Jiyeon Han, Misun Lee, Mingeun Kim, Nahye Park, Jong-Min Suh, Yelim Yi, Gunhee Kim, and Juri Lee.

I would also like to thank to Mi Sook Lim. Because of her assistance, guidance, and support I could finish my work effectively. She made the environment us to focusing on the research and study. Without her hardworking and sacrifice, we could not effectively use the time for research.

I would also like to thank my dissertation committee members Professors Cheol-Min Park and Won young Choe, for taking the precious time and providing helpful comments.

I would also like to thank all collaborators. I would like acknowledge to also acknowledge my collaborators who have helped me carry out the works described in this thesis. Particularly, I would like to express appreciation to Professor Cheol-Min Park, Minjeong Kim, Professor Jaeheung Cho and Dr. Shin Jung Lee who were especially helpful and without their expertise this work would not have been possible.

Lastly, I would love to appreciate my parents, Namil Ji and Namsoon Kang, my grandparents, Jonghak Ji and Ahnsik Kim, my brother Yongmin Ji, and my sister Sooyeon Ji for their support and encouragement during last several years.